Inorganic Chemistry

Article

pubs.acs.org/IC

Palladium(II) Complex of a Redox-Active Amidophenolate-Based *O,N,S,N* Ligand: Its Monocation and Dication and Reactivity with PPh_3

Akram Ali,[†] Suman K. Barman,[†,‡] and Rabindranath Mukherjee*[,†,‡]

[†]Department of Chemistry, Indian Institute of Technology Kanpur, Kanpur 208 016, India

[‡]Department of Chemistry, Indian Institute of Science Education and Research Kolkata, Mohanpur 741 246, India

Supporting Information

ABSTRACT: A new potentially tetradentate redox-active *o*-aminophenol-based ligand, H_2L = 2-(2-ethylthio)pyridine-anilino-4,6-di-*tert*-butylphenol, reacts with $Pd^{II}(O_2CCH_3)_2$ in CH_3OH in the presence of air and Et_3N affording isolation of a green crystalline solid of composition [Pd(L)] **1**. When examined by cyclic voltammetry (CV), **1** exhibits two quasireversible oxidative responses at $E_{1/2}$ = 0.16 (peak-to-peak separation, ΔE_p = 100 mV) and 0.89 V (ΔE_p = 90 mV) vs SCE (saturated calomel electrode). Chemical oxidation of **1** by $[Fe^{III}(\eta^5\text{-}C_5H_5)_2][PF_6]$ and $AgBF_4$ in CH_2Cl_2 led to the isolation of two crystalline solids, red $[Pd(L)][PF_6]\cdot CH_2Cl_2$ **2** and dark green $[Pd(L)][BF_4]_2\cdot 2CH_2Cl_2$ **3**, respectively. Single-crystal X-ray crystallography at 100(2) K unambiguously established that the *O,N,S,N*-coordinated ligand is present in the square-planar complexes $[Pd^{II}\{(L^{AP})^{2-}\}]$ **1**, $[Pd^{II}\{(L^{ISQ})^{\bullet-}\}][PF_6]\cdot CH_2Cl_2$ **2**, and $[Pd^{II}\{(L^{IBQ})^{0}\}][BF_4]_2\cdot 2CH_2Cl_2$ **3**, as dianionic $(L^{AP})^{2-}$, monoanionic *o*-iminobenzosemiquinonate(1−) π-radical (S_{rad} = $^1/_2$) $(L^{ISQ})^{\bullet-}$, and neutral *o*-iminobenzoquinone $(L^{IBQ})^0$ redox level. Reaction of **1** and **2** with PPh_3 afforded isolation of two crystalline complexes: dark green $[Pd^{II}(L)(PPh_3)]$ **4** and red $[Pd^{II}\{(L^{ISQ})^{\bullet-}\}(PPh_3)][PF_6]\cdot CH_2Cl_2$ **5**. X-ray structure determination of **5** at 100(2) K revealed $Pd^{II}ON_2P$ coordination environment. The square-planar complexes **1**−**5** possess an S = 0, $^1/_2$, 0, 0, and $^1/_2$ ground-state, respectively, as was established by ^1H NMR and EPR spectroscopy, and room-temperature magnetic moment data. All redox processes are thus shown to be ligand-based. Absorption spectral measurements were done for all complexes. DFT calculations at B3LYP-level of theory adequately describe the electronic structures of **1**−**3**, and **5**, containing a spin-paired d^8 Pd^{II} ion. Time-dependent-DFT calculations on **1**−**3** and **5** shed light on the origin of UV−vis−NIR spectral absorptions.

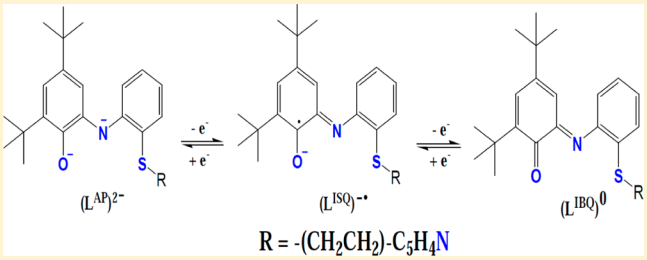

INTRODUCTION

Transition-metal complexes with redox-active ligands have generated much current interest owing to their multielectron redox chemistry and role in catalysis.[1,2] Impetus for this research direction arises from the existence of such systems in the active sites of metalloenzymes.[3−5] Because of the redox-active character these ligands profoundly influence the electronic structural properties of the resulting complexes.[6] Therefore, it is important to have a clear understanding of the bonding and properties of such systems of both biological and synthetic origin to provide a rationale for their reactivity. Much of this research has been reported on complexes containing dioxolenes,[7−9] dithiolenes,[7,10] phenolates,[11] 1,2-bis(pyridine-2-carboxamido)benzene,[7,12] *o*-phenylenediamines,[7,13] salen-/thiosalen-derivatives,[14−17] and *o*-aminophenolates,[7,18−25] *o*-aminothiolates,[7,10] bis(imino)pyridines,[26] and 2-(arylazo)pyridines.[27] A sizable number of new ligands have also been added to this list.[28−32]

o-Aminophenolates[7,18−25] are prototypical redox-active ligands whose abilities to span oxidation levels range from dianionic to monoanionic (iminosemiquinone) to neutral (iminoquinone) forms, allowing them to store redox equivalents. X-ray crystallography has proved to be a powerful tool in determining the oxidation level of the coordinated redox-active ligands. The situation is more complicated in delocalized systems, where the free-electron of the radical ligand is shared between one or more ligands.[6] In such cases, the differences in the metrical parameters for the redox-inactive (closed-shell system) and redox-active (open shell system) forms of the ligand are often small and may not be detectable by X-ray crystallography.[6]

Recently, we reported[33] synthesis, properties, and assignment of correct electronic structure of three low-spin iron(III) complexes of a tridentate redox-active azo-appended *o*-aminophenol-based ligand, 2-(2-phenylazo)-anilino-4,6-di-*tert*-butylphenol, $[Fe^{III}\{(L_{N,N,O})_2\}^{\bullet-}]$ (S = 0), its monocation $[Fe^{III}\{(L^{ISQ})^{\bullet-}\}_2][BF_4]$ (S = $^1/_2$), and its monoanion $[Co^{III}(\eta^5\text{-}C_{10}H_{15})_2][Fe^{III}\{(L^{AP})^{2-}\}_2]$ (S = $^1/_2$). The first two complexes were structurally characterized, and the complexes provided examples of a delocalized system. We provided convincing evidence that valence-tautomerism is operative for the monocation and the monoanion. In our search for a new *o*-aminophenol-based electronically localized tetradentate ligand

Received: December 30, 2014
Published: May 13, 2015

DOI: 10.1021/ic503103e
Inorg. Chem. 2015, 54, 5182−5194

we directed our attention to the synthesis of 2-(2-ethylthio)-pyridine-anilino-4,6-di-*tert*-butylphenol (H_2L; Figure 1). The

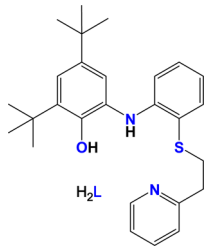

Figure 1. Ligand H_2L.

unique feature of H_2L is that it has a redox-active *o*-aminophenol part and a primarily redox-inactive 2-(2-ethylthio)pyridine part. Inspired by some recent work[19] on redox chemistry of Pd complexes containing redox-active ligands which display ligand-centered redox processes and are employed as catalysts in a huge range of reactions, in this work we have chosen palladium(II) as the metal ion to avoid ligand dissociation during the ligand redox-state shuttling events. We report here on synthesis, structural characterization, and electronic structure of a new diamagnetic complex $[Pd^{II}\{(L^{AP})^{2-}\}]$ (**1**), through absorption and ^{1}H NMR spectral properties, and cyclic voltammetry. We also describe the synthesis and characterization (room-temperature magnetic moment, absorption, EPR, and ^{1}H NMR spectral properties), and elucidation of the electronic structure of the monocation $[\mathbf{1}]^{1+}$ and the dication $[\mathbf{1}]^{2+}$ in the successful synthesis of $[Pd^{II}\{(L^{ISQ})^{\bullet-}\}][PF_6]\cdot CH_2Cl_2$ (**2**) and $[Pd^{II}\{(L^{IBQ})^{0}\}][BF_4]_2\cdot 2CH_2Cl_2$ (**3**), respectively. We report here also the structural properties of **2** and **3**. Reactivity of **1** and **2** toward external substrate (ligand) has been accomplished in the successful synthesis of complexes $[Pd^{II}\{(L^{AP})^{2-}\}(PPh_3)]$ **4** and $[Pd^{II}\{(L^{ISQ})^{\bullet-}\}(PPh_3)][PF_6]\cdot CH_2Cl_2$ **5**, respectively. Complex **5** has been structurally characterized. Density functional theory (DFT) calculation at the B3LYP level of theory has been utilized to assign not only the correct oxidation state of the metal ion but also the oxidation level of the coordinated ligands in each complex. Results of time-dependent (TD) DFT calculations on **1**−**3** and **5** are also presented here throwing light on the origin of absorption spectral absorptions for all the complexes.

EXPERIMENTAL SECTION

General Considerations. All reagents were obtained from commercial sources and used as received. Solvents were dried/purified as reported previously.[33] ([2′-Aminophenylthio]ethyl)pyridine was synthesized following a reported procedure.[34] $[Fe^{III}(\eta^5\text{-}C_5H_5)_2][PF_6]$ was prepared as reported in the literature.[35] Tetra-*n*-butylammonium perchlorate (TBAP) was prepared and purified as before.[33]

Synthesis of H_2L. To a stirring solution of 3,5-di-*tert*-butylcatechol (0.2 g, 0.9 mmol) in *n*-heptane (1 mL) was added a solution of Et_3N (0.12 mL) and ([2′- aminophenylthio]ethyl)pyridine (0.207 g, 0.9 mmol) in *n*-heptane (1 mL), under dinitrogen atmosphere. The reaction mixture was heated to reflux for 6 h. Solvent was then removed under reduced pressure, and the crude mass thus obtained was purified by silica gel column chromatography [ethyl acetate: *n*-hexane; 2:98 (v/v)]. The dark green band was collected to yield the pure ligand as a dark green solid (0.170 g, ∼44%). Anal. Calcd for $C_{27}H_{34}N_2OS$ (H_2L): C 74.61, H 7.88, N 6.45. Found: C 73.78, H 8.02, N 6.90. ^{1}H NMR ($CDCl_3$, 500 MHz): δ (ppm) 1.28 (s, 9H; *tert*-butyl), 1.46 (s, 9H; *tert*-butyl), 3.07−3.10 (m, 2H, $-CH_2-$), 3.24−3.27 (m, 2H, $-CH_2-$), 6.50 (d, J = 7.20 Hz, 1H, Ph-H_{10}), 6.68−6.73 (m, 2H, Ph-H8 and Ph-H_{11}), 6.86 (d, J = 7.34 Hz, 1H, Ph-H_{12}), 7.01 (s, 1H, Ph-H_{15}), 7.09−7.12 (t, d, J = 0.85 Hz, 6.02 Hz, 1H, Ph-H_9), 7.18 (d, J = 7.70 Hz, 1H, Ph-H_7), 7.22 (d, J = 7.08 Hz, 1H, Py-H_4), 7.46 (d, d, J = 1.4 Hz, 7.73 Hz, 1H, Py-H_2), 7.59−7.62 (t, d, J = 1.88 Hz, 7.65 Hz, 1H, Py-H_3), 8.40 (d, J = 4.43 Hz, 1H, Py-H_1). ESI-MS of $C_{27}H_{34}N_2OS$: 435.24 (M^+ +1 ion peak, 100%).

Synthesis of Complexes. *[Pd(L)] (1).* To a suspension of H_2L (0.200 g, 0.46 mmol) in CH_3OH (10 mL) was added Et_3N (0.093 g, 0.93 mmol), and the reaction mixture stirred for 5 min. Then, solid $Pd^{II}(O_2CCH_3)_2$ (0.104 g, 0.46 mmol) was added, and the reaction mixture was refluxed for 4 h. It was then cooled, and the green microcrystalline solid that formed was filtered, washed with CH_3OH, and dried in vacuum. Yield: 0.150 g, ∼60%. Anal. Calcd for $C_{27}H_{32}N_2OSPd$ (**1**): C 60.16, H 5.98, N 5.20. Found: C 60.02, H 6.05, N 5.24. ^{1}H NMR ($CDCl_3$, 500 MHz): δ (ppm) 1.28 (s, 9H; *tert*-butyl), 1.46 (s, 9H; *tert*-butyl), 3.19−3.22 (m, 2H, $-CH_2-$), 3.38−3.41 (m, 2H, $-CH_2-$), 7.06 (m, 2H, Ph-H_8 and Ph-H_{11}), 7.14 (m, 2H, Ph-H_{10} and Ph-H_{12}), 7.18 (d, J = 7.14 Hz, 1H, Ph-H_7), 7.22 (t, J = 7.22 Hz, 1H, Ph-H_9), 7.31 (d, J = 6.98 Hz, 1H, Py-H_4), 7.46 (t, J = 7.14 Hz, 1H, Py-H_2), 7.78 (t, J = 7.45 Hz, 1H, Py-H_3), 9.05 (s, 1H, Py-H_1). The green solid was redissolved in CH_2Cl_2−CH_3OH (6 mL; 1:2 v/v) and left for slow evaporation, affording green crystals suitable for X-ray diffraction studies.

[Pd(L)][PF$_6$]·CH$_2$Cl$_2$ (2). Complex **1** (0.060 g, 0.11 mmol) was dissolved in CH_2Cl_2 (10 mL), and solid $[Fe^{III}(\eta^5\text{-}C_5H_5)_2][PF_6]$ (0.038 g, 0.11 mmol) was added to it. The mixture was stirred at 298 K for 1 h. The solution was then concentrated to ∼2 mL, diethyl ether (6 mL) was added, and the solution was kept in the refrigerator for 1 h. The solid which separated out was filtered off and washed thoroughly with diethyl ether, until the washings were colorless. A red microcrystalline solid was isolated. Yield: 0.060 g, ∼80%. Vapor diffusion of diethyl ether to a CH_2Cl_2 solution of the complex afforded single-crystals suitable for X-ray diffraction of composition $[Pd(L)][PF_6]\cdot CH_2Cl_2$. Anal. Calcd for $C_{28}H_{34}Cl_2F_6N_2OPSPd$ (**2**): C 43.73, H 4.43, N 3.64. Found: C 44.14, H 4.50, N 3.60. IR (KBr, cm^{-1}, selected peak): 841 $\nu(PF_6^-)$.

[Pd(L)][BF$_4$]$_2$·2CH$_2$Cl$_2$ (3). To a solution of **1** (0.060 g, 0.11 mmol) in CH_2Cl_2 (10 mL) was added solid $AgBF_4$ (0.043 g, 0.22 mmol). The mixture was stirred at 298 K for 1 h and then filtered (removal of metallic Ag). The solvent was removed by rotary evaporation under reduced pressure, and the solid that formed was recrystallized from a CH_2Cl_2−*n*-hexane mixture (1:3, v/v). Dark green crystals of composition $[Pd(L)][BF_4]_2\cdot 2CH_2Cl_2$ that formed were found to be suitable for X-ray structural study. Yield: 0.058 g, ∼74%. Anal. Calcd for $C_{29}H_{36}B_2Cl_4F_8N_2OSPd$ (**3**): C 42.16, H 4.30, N 3.51. Found: C 40.01, H 4.13, N 3.50. IR (KBr, cm^{-1}, selected peak): 1052 $\nu(BF_4^-)$. ^{1}H NMR ($CDCl_3$, 500 MHz): δ (ppm) 1.28 (s, 9H; *tert*-butyl), 1.46 (s, 9H; *tert*-butyl), 3.27−3.29 (m, 2H, $-CH_2-$), 3.39−3.41 (m, 2H, $-CH_2-$), 7.02 (m, 2H, Ph-H_8 and Ph-H_{11}), 7.06 (m, 2H, Ph-H_{10} and Ph-H_{12}), 7.12 (d, J = 7.14 Hz, 1H, Ph-H_7), 7.16 (t, J = 7.22 Hz, 1H, Ph-H_9), 7.24 (d, J = 6.98 Hz, 1H, Py-H_4), 7.30 (t, J = 7.14 Hz, 1H, Py-H_2), 7.73 (t, J = 7.45 Hz, 1H, Py-H_3), 9.04 (s, 1H, Py-H_9).

[Pd(L)(PPh$_3$)] (4). To a solution of **1** (0.050 g, 0.09 mmol) in CH_2Cl_2 (10 mL) was added solid PPh_3 (0.024 g, 0.09 mmol). The color of the solution immediately changed from green to dark green. After stirring for 2 h at 298 K, the volume of the solution was reduced to ∼2 mL. Addition of *n*-hexane (10 mL) resulted in the precipitation of a dark green solid, which was collected by filtration, washed with *n*-hexane, and dried in vacuum. Yield: 0.055 g, ∼75%. Anal. Calcd for $C_{45}H_{47}N_2OPSPd$ (**4**): C 67.45, H 5.91, N 3.50. Found: C 66.75, H 5.94, N 3.46. ^{1}H NMR ($CDCl_3$, 500 MHz): δ (ppm) 1.28 (s, 9H; *tert*-butyl), 1.46 (s, 9H; *tert*-butyl), 3.03 (m, 2H, $-CH_2-$), 3.23 (m, 2H, $-CH_2-$), 6.75 (s, 1H, Ph-H_{11}), 6.94 (t, J = 7.45 Hz, 1H, Ph-H_8), 7.02 (m, 2H, Ph-H_{10} and Ph-H_{12}), 7.07 (d, 1H, Ph-H_7), 7.17 (t, 1H, Ph-H_9), 7.35−7.45 (m, 2H, Ph-H_{17} and Py-H_4), 7.54 (t, J = 7.45 Hz, 1H, Py-H_2), 7.66 (t, J = 7.45 Hz, 1H, Ph-H_{16}), 7.78−7.74 (m, 2H, Ph-H_{15} and Py-H_3), 8.35 (d, J = 5.75 Hz 1H, Py-H_1). Electronic spectrum [λ_{max}, nm (ε, M^{-1} cm^{-1})] (in CH_2Cl_2): 650 (575), 424 (2700), 350 (20 750).

DOI: 10.1021/ic503103e
Inorg. Chem. 2015, 54, 5182−5194

Table 1. Data Collection and Structure Refinement Parameters for [Pd(L)] (1), [Pd(L)][PF_6]·CH_2Cl_2 (2), [Pd(L)][BF_4]$_2$·2CH_2Cl_2 (3), and [Pd(L)(PPh_3)][PF_6]·CH_2Cl_2 (5)

	1	2	3	5
formula	$C_{27}H_{32}N_2O_{1.75}PdS$	$C_{28}H_{34}Cl_2F_6N_2OPSPd$	$C_{29}H_{36}B_2Cl_4F_8N_2OSPd$	$C_{46}H_{49}Cl_2F_6N_2OP_2SPd$
fw	551.01	768.90	882.48	1031.17
cryst color, habit	green, block	red, block	green, block	red, block
T/K	100(2)	100(2)	100(2)	100(2)
cryst syst	monoclinic	triclinic	triclinic	monoclinic
space group	$P2_1/c$ (No. 14)	$P\bar{1}$ (No. 2)	$P\bar{1}$ (No. 2)	$P2_1/c$ (No. 14)
a/Å	13.003(3)	10.0900(14)	9.3607(6)	21.153(4)
b/Å	10.137(2)	10.8613(15)	9.9356(7)	11.155(2)
c/Å	18.384(4)	15.041(2)	20.6551(13)	20.546(4)
α/deg	90.0	98.245(2)	103.5100(10)	90.0
β/deg	92.427(4)	101.789(2)	101.0390(10)	105.840(3)
γ/deg	90.0	99.790(2)	94.5950(10)	90.0
V/Å^3	2421.2(17)	1562.7(4)	1817.5(2)	4663.8(17)
Z	4	2	2	4
D_c/g cm^{-3}	1.512	1.634	1.612	1.464
μ/mm^{-1}	0.879	0.945	0.931	0.687
reflns measured	12 593	8399	9827	24 039
unique reflns/R_{int}	4493/0.0540	5684/0.0266	6596/0.0243	8654/0.0426
reflns used [$I > 2\sigma(I)$]	3631	4692	5407	6840
R1,[a] wR2[b] [$I > 2\sigma(I)$]	R1 = 0.0426	R1 = 0.0708	R1 = 0.0524	R1 = 0.0423
	wR2 = 0.0996	wR2 = 0.1932	wR2 = 0.1295	wR2 = 0.0992
R1,[a] wR2[b] (all data)	R1 = 0.0635	R1 = 0.0852	R1 = 0.0678	R1 = 0.0604
	wR2 = 0.1365	wR2 = 0.2179	wR2 = 0.1601	wR2 = 0.1330
GOF on F^2	0.920	1.088	1.067	1.124

[a] $R1 = \sum||F_o| - |F_c||/\sum|F_o|$. [b] $wR2 = \{\sum[w\,(|F_o|^2 - |F_c|^2)^2]/\sum[w(|F_o|^2)^2]\}^{1/2}$.

[Pd(L)(PPh_3)][PF_6]·CH_2Cl_2 (5). To a solution of **2** (0.050 g, 0.07 mmol) in CH_2Cl_2 (10 mL) was added solid PPh_3 (0.019 g, 0.07 mmol). The mixture was stirred at 298 K for 30 min. Solvent was then removed under reduced pressure, and the red solid thus formed was recrystallized from CH_2Cl_2−diethyl ether (1:3, v/v). Red crystals of composition [Pd(L)(PPh_3)][PF_6]·CH_2Cl_2 that formed were found to be suitable for X-ray structural study. Yield: 0.050 g, ∼84%. Anal. Calcd for $C_{46}H_{49}Cl_2F_6N_2OP_2SPd$ (**5**): C 53.58, H 4.79, N 2.72. Found: C 54.06, H 4.85, N 2.75. IR (KBr, cm^{-1}, selected peak): 841 $\nu(PF_6^-)$.

Physical Measurements. Elemental analyses were obtained using Thermo Quest EA1110 CHNS-O, Italy. IR spectra (KBr, 4000−600 cm^{-1}) were recorded on a Bruker Vector 22 spectrophotometer. UV−vis spectra were recorded at 298 K using an Agilent 8453 diode-array spectrophotometer. NIR absorption spectra were recorded using a JACSO V-670 (Japan) spectrophotometer. ^{1}H NMR spectra ($CDCl_3$) were obtained on a JEOL JNM LA 500 (500 MHz) spectrometer. Chemical shifts are reported in ppm referenced to TMS. ESI-MS spectra were recorded on a Waters-HAB213 spectrometer. X-band electron paramagnetic resonance (EPR) spectra were recorded by using a Bruker EMX 1444 EPR spectrometer, fitted with a quartz Dewar for measurement at 77 K, operating at 9.455 GHz. The EPR spectra were calibrated with diphenylpicrylhydrazyl, DPPH (g = 2.0037). Spectra were treated by using the Bruker WinEPR software and simulated using the Bruker SIMFONIA software.

Cyclic voltammetric (CV) experiments were performed at 298 K by using CH Instruments Electrochemical Analyzer/Workstation model 600B series. The cell contained a Beckman M-39273 platinum-inlay working electrode, a Pt wire auxiliary electrode, and a saturated calomel electrode (SCE), as reference electrode. Details of the cell configuration are as described before.[33] For coulometry, a platinum wire-gauze was used as the working electrode. The solutions were ∼1.0 mM in complex and 0.1 M in supporting electrolyte, TBAP.

Under our experimental conditions, the $E_{1/2}$ and peak-to-peak separation (ΔE_p) values in CH_2Cl_2 for [$Fe^{III}(\eta^5$-$C_5H_5)_2$]$^+$/[$Fe^{II}(\eta^5$-$C_5H_5)_2$] (Fc^+/Fc) couple were 0.49 V vs SCE and 120 mV, respectively.[33]

Room-temperature magnetic susceptibility measurements were made on polycrystalline samples (powder form) of [Pd(L)][PF_6]·CH_2Cl_2 **2** and [Pd(L)(PPh_3)][PF_6]·CH_2Cl_2 **5** by the Faraday method, using a locally built magnetometer.[36] The effective magnetic moment was calculated from $\mu_{eff} = 2.828[\chi_M T]^{1/2}$, where χ_M is the corrected molar susceptibility. The diamagnetic corrections were applied to the susceptibility data.[37] Solution-state magnetic susceptibilities were obtained by the NMR technique of Evans[38] in CH_2Cl_2 with a JEOL JNM LA 500 (500 MHz) spectrometer and made use of the paramagnetic shift of the methylene protons of CH_2Cl_2 as the measured NMR parameter.

X-ray powder diffraction (XRPD) of **1**, **2**, **3**, and **5** were recorded with a bruker D8 Advance Series-2 powder X-ray diffractometer, operated at 40 kV and 40 mA, using a Cu-target tube and a graphite monochromator. The intensity data were recorded by continuous scan in a $2I/I$ mode from 6° to 50° with a step size of 0.05° and a scan speed of 3° min^{-1}. Simulation of the XRPD spectra was carried out by the single-crystal data and diffraction-crystal module of the Mercury (Hg) program available free of charge via the Internet at http://www.iucr.org.

Crystal Structure Determination. Single-crystals of suitable dimensions were used for data collection. Diffraction intensities were collected on a Bruker SMART APEX CCD diffractometer, with graphite-monochromated Mo Kα (λ = 0.710 73 Å) radiation at 100(2) K. The data were corrected for absorption. The structures were solved by SIR-97, expanded by Fourier-difference syntheses, and refined with SHELXL-97 incorporated in WinGX 1.64 crystallographic package.[39] The positions of the hydrogen atoms were calculated by assuming ideal geometries, but not refined. All non-hydrogen atoms were refined with anisotropic thermal parameters by full-matrix least-squares procedures on F^2.

For **1**, in the coordinated L(2−) the occurrence of partial thioether oxidation was realized during the crystal structure determination. After several runs, the optimum value for the occupancy of O atom has been fixed at 0.8. Since it is not affecting our chemistry, we did not probe any further about the correct occupancy value. It seems, however, that the occupancy should be more than 0.6. We confirmed that it

DOI: 10.1021/ic503103e
Inorg. Chem. 2015, 54, 5182−5194

Scheme 1

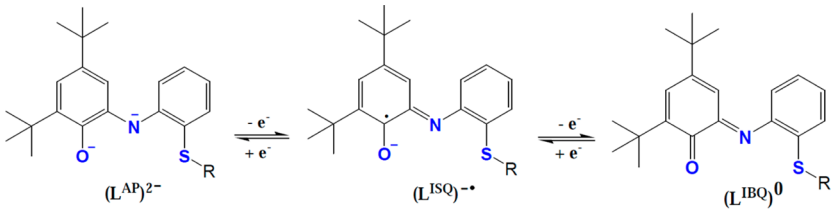

happened during the recrystallization step. In spite of our sincere attempts we could not grow single-crystals of **1**, without formation of partial oxidation of thioether sulfur. Pertinent crystallographic parameters are summarized in Table 1. CCDC-1032420 (**1**), 1032421 (**2**), 1032422 (**3**), and 1032423 (**5**) contain the supplementary crystallographic data for this paper. These data can be obtained free of charge from The Cambridge Crystallographic Data Centre via www.ccdc.cam.ac.uk/data_request/cif.

Computational Details. All DFT calculations were performed using the Gaussian 09 program[40] with B3LYP functional.[41] Hay and Wadt basis set LANL2DZ with pseudopotential[42] was employed for palladium. Triple-ζ quality basis sets (TZVP)[43] were used for sulfur, oxygen, and nitrogen while the SVP basis set[44] was used for all other atoms. TD-DFT calculations were done employing the B3LYP functional and the polarizable continuum model, CPCM (CH_2Cl_2 as solvent).[45] TD-DFT-derived electronic spectra were plotted using GaussSum.[46] Corresponding orbitals and spin-density plots were made using Chemcraft[47] Visualization program. EPR parameters were calculated with the optimized geometry at the same level of theory and same basis sets.

RESULTS AND DISCUSSION

Synthesis of New Ligand H_2L and the Complex [Pd(L)] 1. The tetradentate ligand H_2L was synthesized following the procedure reported earlier by our group.[33] Stoichiometric reaction of 3,5-di-*tert*-butylcatechol with ([2′-aminophenylthio]ethyl)pyridine in the presence of Et_3N, in *n*-heptane under dinitrogen atmosphere, leads to the isolation of a crude ligand. This was further purified by silica gel column chromatography [ethyl acetate/*n*-hexane; 2:98 (v/v)] to isolate the pure ligand H_2L as a green solid, which was characterized by ^{1}H NMR (Figure S1, Supporting Information) and ESI-MS spectra (Figure S2, Supporting Information).

Preparation of a mononuclear palladium(II) complex containing a *O*,*N*,*S*,*N*-coordinated tetradentate ligand H_2L, in its deprotonated form, has been performed in a straightforward manner in CH_3OH by the reaction of $Pd^{II}(O_2CCH_3)_2$, H_2L, and Et_3N as a base in the presence of air at refluxing temperature. A green microcrystalline solid of composition [Pd(L)] **1** was obtained in a moderate yield, which was correctly analyzed by elemental analysis. Complex **1** exhibits in $CDCl_3$ a clean ^{1}H NMR spectrum in the δ 0−10 ppm range, attesting to its diamagnetic character (Figure S3, Supporting Information). Positive ESI-MS of [Pd(L)] in CH_2Cl_2 showed a peak at m/z = 539.13 corresponding to the species {[Pd(L)] + H^+}, on the basis of the simulated mass and isotopic distribution pattern (Figure S4, Supporting Information). Recrystallization of the microcrystalline solid from CH_2Cl_2−CH_3OH resulted in X-ray quality single-crystals. Notably, recrystallization of **1** (slow evaporation in air) resulted in the oxidation of thioether sulfur (see below; crystal structure). We did not investigate this aspect[48] any further.

Redox Properties of 1. *o*-Amidophenolates(2−) are redox-active and can exist in three redox levels,[5,7,18−24] and Scheme 1 shows the geometric and electronic features observed.

To investigate the possibility of identifying metal-centered redox and/or accessibility of various ligand redox levels, CV experiments on **1** were carried out. The CV of **1** in CH_2Cl_2 displays (Figure 2) two oxidative redox processes at $E_{1/2}$ values

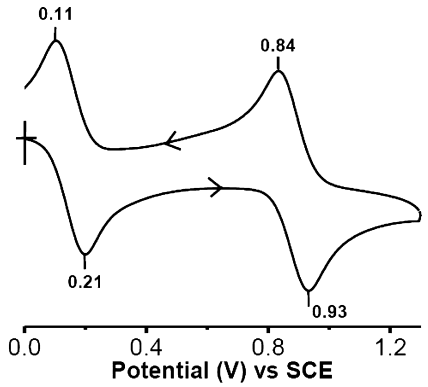

Figure 2. Cyclic voltammogram (100 mV/s) of a 1.0 mM solution of [Pd(L)] **1** in CH_2Cl_2 (0.1 M in TBAP) at a platinum working electrode. Indicated peak potentials are in V vs SCE.

of 0.16 V (ΔEp = 100 mV) and 0.89 V (ΔEp = 90 mV) vs SCE. Both the oxidation processes are chemically reversible (ratio of cathodic and anodic peak current, $i_{pc}/i_{pa} \approx 1$) and electrochemically quasireversible electron-transfer reactions.[33]

Synthesis and Characterization of $[Pd(L)][PF_6]\cdot CH_2Cl_2$ 2 and $[Pd(L)][BF_4]_2\cdot 2CH_2Cl_2$ 3. One-electron oxidized counterpart of [Pd(L)] **1**, $[Pd(L)][PF_6]\cdot CH_2Cl_2$ **2**, was synthesized as a red microcrystalline solid by stoichiometric chemical oxidation of **1** in CH_2Cl_2 by $[Fe^{III}(\eta^5\text{-}C_5H_5)_2][PF_6]$ ($E_{1/2}$ = 0.40 V vs SCE)[49] at room-temperature. Isolation of two-electron oxidized product of [Pd(L)], $[Pd(L)][BF_4]_2\cdot 2CH_2Cl_2$ **3**, as dark green crystals, was achieved by chemical oxidation of **1** in CH_2Cl_2 by $AgBF_4$ ($E_{1/2}$ = 1.05 V vs SCE)[49] at room-temperature. The composition of **2** and **3** was established by elemental analysis. While **2** is paramagnetic with respect to one-unpaired electron [μ_{eff} (solid, 298 K) = 1.89 μ_B; μ_{eff} (CH_2Cl_2, 300 K) = 1.84 μ_B], **3** is diamagnetic. As a consequence, complex **3** exhibits in $CDCl_3$ a clean ^{1}H NMR spectrum in the δ 0−10 ppm range (Figure S5, Supporting Information). Positive ESI-MS of **2** in CH_2Cl_2 showed a peak at m/z = 538.13 corresponding to the species $[Pd(L)]^+$, on the basis of the simulated mass and isotopic distribution pattern (Figure S6, Supporting Information). Positive ESI-MS of **3** in CH_2Cl_2 showed a peak at m/z = 538.13 corresponding to the species $\{[Pd(L)]^{2+} + e^-\}^+$ (Figure S7, Supporting Information). When examined by CV, **2** displays a one-electron oxidative

DOI: 10.1021/ic503103e
Inorg. Chem. 2015, 54, 5182−5194

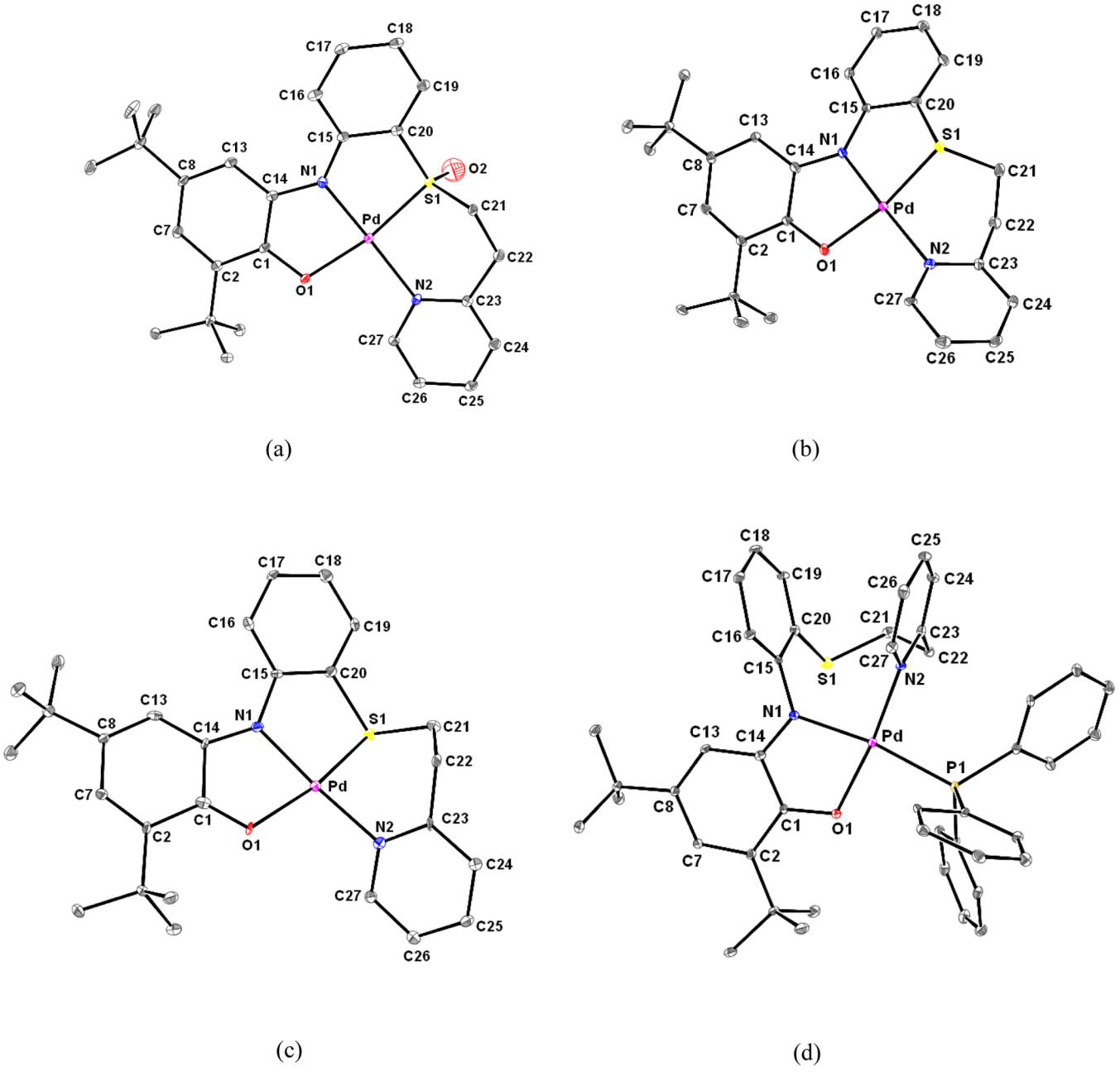

Figure 3. Perspective view of the metal coordination environment in (a) $[Pd^{II}(L)]$ **1**, (b) $[Pd^{II}(L)][PF_6]\cdot CH_2Cl_2$ **2**, (c) $[Pd^{II}(L)][BF_4]_2\cdot 2CH_2Cl_2$ **3**, and (d) $[Pd(L)(PPh_3)][PF_6]\cdot CH_2Cl_2$ **5**.

response and a one-electron reductive response (Figure S8, Supporting Information), and **3** displays two-reductive (Figure S9, Supporting Information) one-electron redox responses, as expected.

Complexes $[Pd(L)]$ **1**, $[Pd(L)][PF_6]\cdot CH_2Cl_2$ **2**, and $[Pd(L)][BF_4]_2\cdot 2CH_2Cl_2$ **3** constitute a three-member electron-transfer series. Thus, complexes **1**−**3** are ideally suited to distinctly distinguish the geometrical and spectroscopic features of the *O*,*N*,*S*,*N*-coordinated, closed-shell, diamagnetic *o*-amidophenolate $(L^{AP})^{2-}$, the corresponding open-shell *o*-iminobenzosemiquinonate(1−) π-radical $(L^{ISQ})^{\bullet -}$ ($S_{rad} = {}^1/_2$), and the closed-shell *o*-iminobenzoquinone $(L^{IBQ})^0$.

Reactivity of 1−3 with PPh_3. To investigate the reactivity potential of **1** toward externally added substrates, the reaction between **1** and PPh_3 in CH_2Cl_2 was carried out. Following usual workup we could isolate a crystalline dark green solid of composition $[Pd(L)(PPh_3)]$ **4**. Complex **4** exhibits in $CDCl_3$ a clean ^1H NMR spectrum in the δ 0−10 ppm range, attesting to its diamagnetic character (Figure S10, Supporting Information). Notably, the doublet at δ 8.35 ppm could be assigned due to Py-H_1. Given the δ value for Py-H_1 for free ligand at 8.40 ppm and for **1** at 9.05 ppm, we are inclined to believe that the pyridine of ethylpyridine arm is not coordinated. In fact, the signals for two methylene protons of the −S−CH_2−CH_2−S− moiety of **4** (3.03 and 3.23 ppm) are distinctly different from that observed for **1** (3.19−3.22 and 3.38−3.41 ppm) but closely similar (thioether S is coordinated but not pyridine) to that observed for free H_2L (3.07−3.10 and 3.24−3.27 ppm). Positive ESI-MS of **4** in CH_2Cl_2 showed a peak at m/z = 801.22 corresponding to the species $\{[Pd(L)(PPh_3)] + H^+\}$, on the

DOI: 10.1021/ic503103e
Inorg. Chem. 2015, 54, 5182−5194

Table 2. Selected Bond Lengths (Å) and Bond Angles (deg) in [Pd(L)] (1), [Pd(L)][PF_6]·CH_2Cl_2 (2), [Pd(L)][BF_4]$_2$·2CH_2Cl_2 (3), and [Pd(L)(PPh_3)][PF_6]·CH_2Cl_2 (5)

Bond Lengths (Å)							
1		2		3		5	
Pd–N1	1.957(4)	Pd–N1	1.965(5)	Pd–N1	1.978(4)	Pd–N1	2.043(3)
Pd–N2	2.075(4)	Pd–N2	2.035(5)	Pd–N2	2.022(4)	Pd–N2	2.027(3)
Pd–O1	2.004(4)	Pd–O1	2.018(5)	Pd–O1	2.062(4)	Pd–O1	2.001(3)
Pd–S1	2.198(2)	Pd–S1	2.2248(18)	Pd–S1	2.2195(14)	Pd–P1	2.2848(11)
C1–O1	1.367(6)		1.312(8)		1.252(6)		1.318(5)
C14–N1	1.398(7)		1.372(9)		1.316(7)		1.347(5)
C15–N1	1.389(7)		1.414(8)		1.417(7)		1.416(5)
C20–S1	1.776(5)		1.805(7)		1.801(6)		1.769(4)
C21–S1	1.796(5)		1.820(8)		1.835(6)		1.814(4)
C23–N2	1.356(6)		1.332(9)		1.343(7)		1.361(5)
C27–N2	1.354(7)		1.354(9)		1.358(7)		1.354(5)
C1–C2	1.396(7)		1.425(9)		1.457(8)		1.423(6)
C2–C7	1.398(7)		1.355(9)		1.332(7)		1.392(6)
C7–C8	1.389(7)		1.424(10)		1.469(7)		1.436(6)
C8–C13	1.386(7)		1.382(10)		1.355(8)		1.353(6)
C13–C14	1.413(7)		1.411(9)		1.406(7)		1.426(6)
C1–C14	1.413(7)		1.456(9)		1.531(7)		1.444(6)
C15–C16	1.411(7)		1.359(9)		1.398(7)		1.388(6)
C16–C17	1.398(7)		1.401(10)		1.382(8)		1.390(6)
C17–C18	1.387(8)		1.397(10)		1.386(8)		1.359(6)
C18–C19	1.387(7)		1.361(10)		1.397(8)		1.383(6)
C19–C20	1.386(8)		1.376(10)		1.381(8)		1.406(6)
C15–C20	1.410(7)		1.421(9)		1.406(8)		1.391(6)
C21–C22	1.508(7)		1.510(11)		1.536(8)		1.532(6)
C22–C23	1.528(7)		1.528(10)		1.505(8)		1.495(6)
C23–C24	1.384(7)		1.383(10)		1.383(8)		1.387(6)
C24–C25	1.379(7)		1.398(11)		1.372(8)		1.380(6)
C25–C26	1.397(7)		1.381(12)		1.377(8)		1.380(6)
C26–C27	1.364(7)		1.387(10)		1.361(8)		1.365(6)
Bond Angles (deg)							
1		2		3		5	
N1–Pd–O1	83.36(15)		82.9(2)		81.00(16)	N1–Pd–O1	81.46(12)
N1–Pd–N2	172.62(17)		176.1(2)		173.96(18)	N1–Pd–N2	92.72(13)
O1–Pd–N2	95.47(15)		98.1(2)		99.99(15)	O1–Pd–N2	172.08(13)
N1–Pd–S1	86.73(13)		87.44(16)		88.79(14)	N1–Pd–P1	171.20(10)
O1–Pd–S1	169.50(10)		169.54(14)		168.36(10)	O1–Pd–P1	90.01(8)
N2–Pd–S1	94.80(12)		91.84(16)		90.74(13)	N2–Pd–P1	95.57(10)
C20–S1–Pd	98.02(18)		95.5(2)		94.96(19)	C40–P1–Pd	109.67(13)
C21–S1–Pd	98.61(18)		104.7(3)		103.09(19)	C34–P1–Pd	109.66(13)
C1–O1–Pd	110.60(3)		110.2(4)		110.4(3)	C1–O1–Pd	113.0(2)
C14–N1–Pd	112.30(3)		112.8(4)		115.4(4)	C14–N1–Pd	112.2(3)
C15–N1–Pd	117.30(3)		117.8(4)		115.6(3)	C15–N1–Pd	125.0(3)
C23–N2–Pd	126.70(3)		119.9(5)		118.9(4)	C23–N2–Pd	124.6(3)
C27–N2–Pd	114.10(3)		119.4(5)		120.8(4)	C27–N2–Pd	116.2(3)

basis of the simulated mass and isotopic distribution pattern (Figure S11, Supporting Information). Characterization data (Experimental Section) corresponds to the formulation [Pd^{II}{$(L^{AP})^{2-}$}(PPh_3)] **4**. The Lewis acidic Pd^{II} center in **1** can therefore bind an additional ligand, with concomitant coordination environment switching over from Pd^{II}ONSN (**1**) to Pd^{II}ONSP (**4**), however, keeping four-coordination around Pd^{II} invariant. Complexes **1** and **4** provide examples of coordination flexibility. When examined by CV, complex **4** displays two one-electron oxidative responses (Figure S12, Supporting Information). Unfortunately, we have not so far successfully grown X-ray quality single-crystals of **4** for structural characterization.

Oxidation of a metal-bound redox-active ligand is expected to enhance reactivity at the metal center and thus make it susceptible to chemical reactions. In fact, oxidation of **1** to **2** leads to the oxidation of Pd^{II}-coordinated $(L^{AP})^{2-}$ to Pd^{II}-coordinated $(L^{ISQ})^{\bullet-}$ which implies an indirect increase in the Lewis acidity of the Pd^{II} center. The Lewis acidic Pd^{II} center in **2** can therefore bind an additional ligand. In fact, in our pursuit to demonstrate such a reactivity we reacted **2** with PPh_3 in CH_2Cl_2. Interestingly, from such a reaction medium we could isolate a crystalline red solid of composition [Pd(L)(PPh_3)]-[PF_6]·CH_2Cl_2 **5**, which has also been structurally characterized. Positive ESI-MS of **5** in CH_2Cl_2 showed a peak at m/z = 800.22 corresponding to the species $[Pd(L)(PPh_3)]^+$, on the basis of

DOI: 10.1021/ic503103e
Inorg. Chem. 2015, 54, 5182–5194

Table 3. Comparison of X-ray Determined Experimental Bond Lengths with the Calculated Bond Lengths (in Brackets) from Metrical Oxidation State (MOS) Values of 1, 2, 3, and 5

	1	2	3	5
C1−C14	1.413(7) [1.412]	1.456(9) [1.439]	1.531(7) [1.510]	1.444(6) [1.442]
C13−C14	1.413(7) [1.393]	1.411(9) [1.410]	1.406(7) [1.433]	1.426(6) [1.412]
C8−C13	1.386(7) [1.394]	1.382(10) [1.373]	1.355(8) [1.347]	1.353(6) [1.372]
C7−C8	1.389(7) [1.392]	1.424(10) [1.425]	1.469(7) [1.467]	1.436(6) [1.427]
C2−C7	1.398(7) [1.402]	1.355(9) [1.380]	1.332(7) [1.352]	1.392(6) [1.378]
C1−C2	1.396(7) [1.400]	1.425(9) [1.424]	1.457(8) [1.455]	1.423(6) [1.426]
C1−O1	1.367(6) [1.361]	1.312(8) [1.307]	1.252(6) [1.239]	1.318(5) [1.304]
C14−N1	1.398(7) [1.398]	1.372(9) [1.354]	1.316(7) [1.298]	1.347(5) [1.350]

the simulated mass and isotopic distribution pattern (Figure S13, Supporting Information). We have also investigated the reaction of PPh_3 with **3**. Even though we noticed a reaction, initial experiments suggest that the reaction is not at all straightforward and leads to a mixture of products. We have not investigated this reaction any further.

Description of the Structures of [Pd(L)] (1), [Pd(L)][PF_6]·CH_2Cl_2 (2), [Pd(L)][BF_4]$_2$·$2CH_2Cl_2$ (3), and [Pd(L)(PPh$_3$)][PF_6]·CH_2Cl_2 (5). Crystal structure analysis on **1**−**3** confirms that each complex has the tetradentate *O*,*N*,*S*,*N*-donor ligand coordinated to Pd by utilizing all its donor sites. Complexes **2** and **3** contain a PF_6^- anion and two BF_4^- anions and one and two molecules of CH_2Cl_2, as solvent of crystallization, respectively. The metal coordination environments in **1**, **2**, and **3** are displayed in Figure 3 and identified by Pd−O1(phenolate), Pd−N1(amidate/iminate), Pd−N2 (pyridine), and Pd−S1(thioether) distances, respectively: 2.004(4), 1.957(4), 2.075(4), and 2.2000(14) Å for **1**; 2.018(5), 1.965(5), 2.035(5), and 2.2248(18) Å for **2**; 2.062(4), 1.978(4), 2.022(4), and 2.2195(14) Å for **3**. Relevant metric parameters are in Table 2. The Pd−O1(phenolate) and Pd−N1(amidate/iminate) distances monotonically increase, and Pd−N2(pyridine) distances monotonically decrease, with increase in subsequent one-electron oxidation level of the coordinated ligand (see below). The Pd−S distance in **1** is the shortest, given the distances in **2** and **3**. The palladium is present in its bivalent state, as evidenced by closely similar distances in Pd^{II} complexes of *N*,*O*-coordinated *o*-amidophenolates in different oxidation levels.[20f,k] Similar to **1** a neutral complex of Pd^{II} with a *N*,*O*-coordinated *o*-amidophenolate [$(L^{AP}_{N,O})^{2-}$ = 2-(2-trifluoromethyl)anilino-4,6-di-*tert*-butylphenol] and a *N*,*N*-coordinated substituted bpy (4,4′-di-*tert*-butyl-2,2′-bipyridine) has been reported by Wieghardt and coworkers.[20k]

The sensitive C−O and C−N bond distances (Scheme 1) associated with the coordinated ligand in **1** are C1−O1 1.367(5) and C14−N1 1.399(6) Å. Intraring bond distances are C1−C2 1.395(7), C2−C7 1.397(7), C7−C8 1.388(7), C8−C13 1.386(7), C13−C14 1.410(7), and C14−C1 1.415(7) Å, indicating the aromatic, closed-shell character of this phenyl ring. The presence of the Pd^{II} ion, the neutral nature of **1**, the set structural benchmark for C−O and C−N bond distances[5,7,18−24] for three oxidation levels of the ligand (Scheme 1), and the observed parameters, however, suggest that the ligand is coordinated in its diamagnetic dianionic *o*-amidophenolate oxidation level $(L^{AP})^{2-}$. Relevant C−O and C−N distances for **2** are C1−O1 1.312(8) and C14−N1 1.372(9) Å and for **3** are C1−O1 1.252 (6) and C14−N1 1.316(7) Å. Intraring bond distances follow the trend (a "quinoidal" distortion of the aromatic ring with the adjacent long−short−long−short C−C bonds) as mentioned for metal-coordinated *o*-iminosemiquinonate(1−) π-radical $(L^{ISQ})^{\bullet-}$ and *o*-iminobenzoquinone $(L^{IBQ})^0$, respectively [C1−C2 1.425 (9), C2−C7 1.355(9), C7−C8 1.424(10), C8−C13 1.382(10), C13−C14 1.411(9), and C14−C1 1.456(9) Å for **2**; C1−C2 1.457(8), C2−C7 1.332(7), C7−C8 1.469(7), C8−C13 1.355(8), C13−C14 1.406(7), and C14−C1 1.531(7) Å for **3**].

Metric parameters for the *O*,*N*,*S*,*N*-coordinated ligand are noticeably different in the structures of **1**, **2**, and **3**. Thus, the X-ray crystallographic data strongly support the formulation of **1** as $[Pd^{II}\{(L^{AP})^{2-}\}]$, **2** as $[Pd^{II}\{(L^{ISQ})^{\bullet-}\}][PF_6]\cdot CH_2Cl_2$, and **3** as $[Pd^{II}\{(L^{IBQ})^0\}][BF_4]_2\cdot 2CH_2Cl_2$. This assignment rationalizes the absorption spectral features of **1**−**3**.

For **1** the thioether oxidation (Figure 3a) is discussed only briefly (see Crystal Structure Determination subsection of the Experimental Section and Synthesis of [Pd(L)] subsection of Results and Discussion). The following comment on the Pd−S bond lengths for **1**−**3** is in order. The relevant distance is the shortest in **1** (see above). As a consequence of comparatively more electron donation by thioether S to Pd^{II} in **1**, the sulfur center of $(L^{AP})^{2-}$ becomes prone to nucleophilic attack. This could be a plausible reason for observation of partial thioether sulfur oxidation of coordinated L(2−) in **1**.

Complex **5** has only *O*,*N*,*N*-donor sites of L(2−) coordinated, and thioether sulfur does not take part in coordination (Figure 3). The monocationic complex has a PF_6^- counteranion and a CH_2Cl_2 molecule, as solvent of crystallization. The metal coordination environment of **5** is identified by Pd−O1(phenolate), Pd−N1(iminate), Pd−N2-(pyridine), and Pd−P distances, respectively: 2.001(3), 2.043(3), 2.027(3), and 2.2848(11) Å. Relevant metric parameters are in Table 2. We note that in going from **2** to **5** a decrease in the Pd−O1 distance by ∼0.02 Å is observed, a measurable increase (∼0.08 Å) in the Pd−N1 distance, and the Pd−S bond is replaced by the Pd−P bond, with an increase (0.06 Å) in the metal−ligand distance. In **5**, the bond parameters of this *O*,*N*,*N*,*P*-coordinated ligand show C1−01 and C14−N1 distances 1.318(5) and 1.347(5) Å, respectively. As that observed in **2**, a quinoidal distortion of the aromatic ring [C1−C2 1.423(6), C2−C7 1.392(6), C7−C8 1.436(6), C8−C13 1.353(6), C13−C14 1.426(6), and C14−C1 1.444(6) Å] is observed. The aromatic ring is assigned as *o*-iminobenzosemiquinonate(1−) π-radical anion $(L^{ISQ})^{\bullet-}$. The assignment of **5** as $[Pd^{II}\{(L^{ISQ})^{\bullet-}\}(PPh_3)][PF_6]\cdot CH_2Cl_2$ rationalizes its absorption spectral feature, which closely resembles that of **2** (see Absorption Spectra). This assignment renders the palladium ion divalent.

To the best of our knowledge, complex **5** provides the first example of an externally added ligand (substrate)-bound metal complex of a redox-active ligand with concomitant ligand

DOI: 10.1021/ic503103e
Inorg. Chem. 2015, 54, 5182−5194

coordination sphere rearrangement, without ligand dissociation. Such a binding has been proposed previously.[13d,25a,50] Notably, Weinstein, Sarkar, and co-workers have recently reported[25b] a closely similar reactive Pt^{II} complex with PPh_3 (structurally characterized). However, in this case one of the bidentate coligands (phenylazopyridine) was replaced by two PPh_3 molecules. From a coordination sphere flexibility point of view complex **5** deserves a special mention.

Metrical Oxidation States (MOSs) of Ligands in Complexes 1−3 and 5. Recently in an attempt to quantitatively determine the redox level of redox-active ligands, Brown et al. proposed the MOS concept,[24b] based on least-squares fitting of relevant C−O, C−N, and C−C bond lengths. By this approach, using X-ray determined metrical parameters one can determine the empirical oxidation state of ligands. Using this concept the MOS of the ligand in complex **1** is calculated as −1.92 ± 0.09, which is consistent with the dianionic form (2−) of the ligand. Using this MOS value of −1.92, the C1−O1 and C14−N1 bond distances are calculated as 1.361 and 1.398 Å, respectively, which are in excellent agreement with the X-ray determined values of 1.367 and 1.399 Å. Similarly, for complexes **2**, **3**, and **5** the MOS values are calculated as −1.08 ± 0.13, −0.01 ± 0.13, and −1.02 ± 0.11, respectively. These values are consistent with the proposed redox-level of ligands in respective complexes. Table 3 describes the comparison of MOS-derived calculated bond lengths and X-ray metrical parameters of relevant atoms.

X-ray Powder Diffraction (XRPD). To extract information about the qualitative indicator of purity of bulk samples X-ray powder diffraction analyses were also performed. The experimental and computer simulated XRPD patterns of **1**, **2**, **3**, and **5** are shown in Figures S14, S15, S16, S17, Supporting Information, respectively. Although for **1** the experimental pattern has a few unindexed diffraction lines in comparison with those simulated, it still can confidently be claimed that the bulk sample of **1** is a phase pure complex.

Electronic Structural Aspects: DFT Results. Assignment of correct oxidation level of the coordinated ligand and the oxidation state of Pd in **1**−**3** and **5** has been done by DFT calculations at the B3LYP level of theory (see Computational Details in the Experimental Section). Geometry-optimization of **1** with $S = 0$ ground-state (closed-shell configuration) was computed (Table S1, Supporting Information) to obtain the $[Pd^{II}\{(L^{AP}{}_{O,N,S,N})^{2-}\}]$ electronic configuration (see Crystal Structure section). The calculated ground-state geometry well-reproduced that found in the crystal structure (overall square-planar geometry of **1**) with the exception of the $Pd^{II}-L_{O,N,S,N}$ bond distances, which are ca. 0.02−0.07 Å longer than the experimental value (Table 2 and Table S2, Supporting Information). Notably, the bond distances associated with the ligand-backbone accurately reproduce the oxidation level of the coordinated ligand $(L^{AP})^{2-}$. Selective orbital contour plots for **1** are displayed in Figure 4.

For the one-electron oxidized form of **1**, $[\mathbf{1}]^{1+}$ ($S = {}^1/_2$ ground-state), the geometry-optimization (Table S3, Supporting Information) accurately reproduced the overall square-planar geometry of $[\mathbf{1}]^{1+}$ and bond distances associated with ligand-backbone $(L^{ISQ}{}_{O,N,S,N})^{\bullet-}$ to obtain the $[Pd^{II}\{(L^{ISQ}{}_{O,N,S,N})^{\bullet-}\}]^{1+}$ electronic configuration (see Crystal Structure section). Like that observed for **1**, the $Pd^{II}-L_{O,N,S,N}$ bond distances are longer than the experimental value by ca. 0.02−0.10 Å (Table 2 and Table S2, Supporting Information). Spin-density plot for $[\mathbf{1}]^{1+}$ and qualitative MO diagram of the magnetic orbital are in Figure 5. Geometry optimization (Table S4, Supporting Information) of two-electron oxidized form of

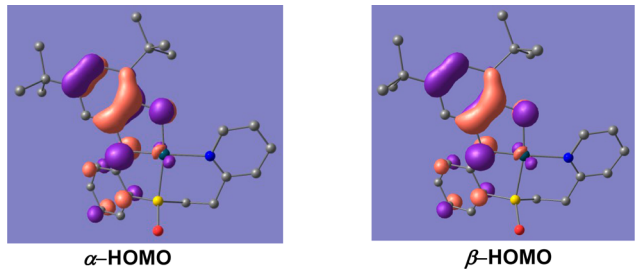

Figure 4. Qualitative MO diagram of the magnetic orbital plot for $[Pd^{II}\{(L^{AP})^{2-}\}]$ **1**.

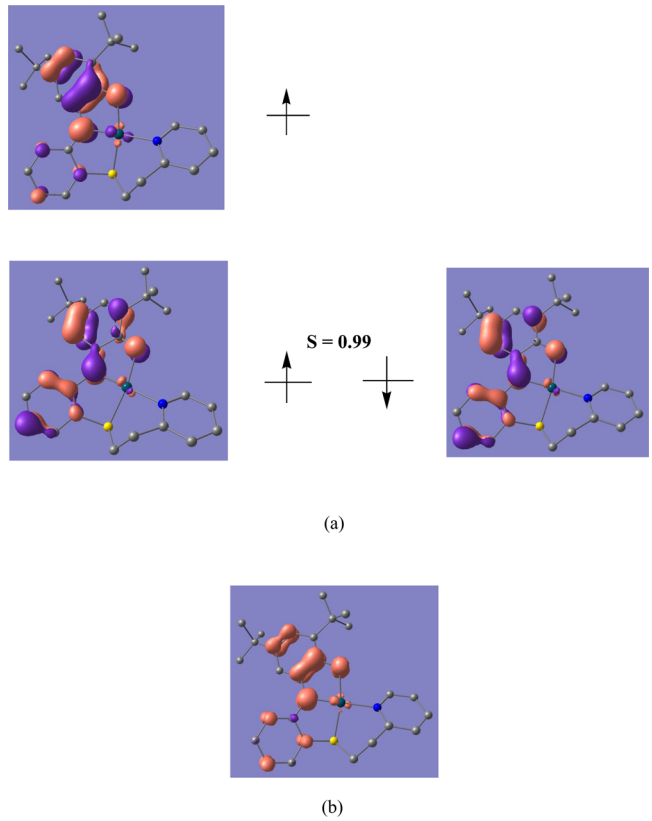

Figure 5. (a) Qualitative MO diagram of the magnetic orbitals and (b) spin-density plot of $[\mathbf{1}]^{1+}$.

1, $[\mathbf{1}]^{2+}$ with $S = 0$ ground-state (closed-shell configuration) accurately reproduced the $[Pd^{II}\{(L^{IBQ}{}_{O,N,S,N})^{0}\}]^{2+}$ electronic configuration (see Crystal Structure section). Here also the $Pd^{II}-L_{O,N,S,N}$ bond distances are longer than the experimental value by ca. 0.04−0.08 Å (Table 2 and Table S2, Supporting Information). For **5**, as for that of $[\mathbf{1}]^{1+}$, geometry-optimization (Table S5, Supporting Information) with $S = {}^1/_2$ ground-state accurately reproduced the overall square-planar geometry of **5** and reproduced the $[Pd^{II}\{(L^{ISQ}{}_{O,N,N})^{0}\}(PPh_3)]^{1+}$ electronic configuration (see Crystal Structure section). The computed and experimental $(L^{ISQ}{}_{O,N,N})^{\bullet-}$ bond distances associated with the ligand-backbone are in good agreement with experimental metrical parameters (Table 2 and Table S6, Supporting Information). Spin-density plot and qualitative MO diagram of the magnetic orbital for **5** are in Figure 6. Thus, it is evident that the observed one-electron redox processes of the series are

DOI: 10.1021/ic503103e
Inorg. Chem. 2015, 54, 5182−5194

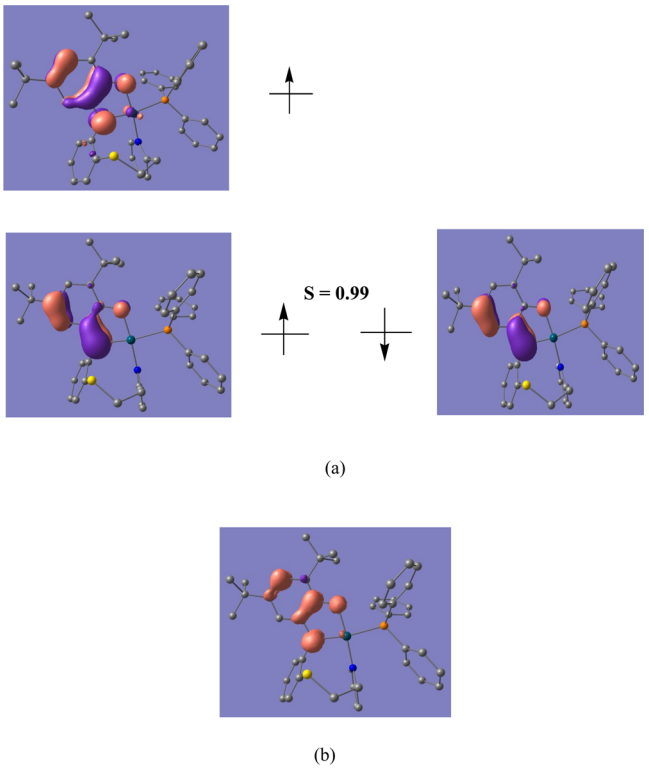

Figure 6. (a) Qualitative MO diagram of the magnetic orbital for **5** and (b) spin-density plot for **5**.

ligand-centered, and the coordinated ligands are present in three oxidation levels $(L^{AP})^{2-}$, $(L^{ISQ})^{\bullet-}$, and $(L^{IBQ})^{0}$ in **1**, **2**, and **3**, respectively. This ligand oxidation level description renders the Pd ion to remain constant at the bivalent state (d^8, $S_{Pd} = 0$). The C−O and C−N bond distances are in good agreement with the oxidation level of the coordinated ligands. For $[\mathbf{1}]^{1+}$ and **4**, and $[\mathbf{1}]^{2+}$, the intraring C−C distances exhibit close agreement with the benchmark set[5,7,18−24] for the $(L^{ISQ})^{\bullet-}$ and $(L^{IBQ})^{0}$ oxidation levels of the *o*-amidophenolate ligands.

Electronic Structural Aspects: EPR Spectra. X-band EPR spectra (298 K as well as at 120 K) of the monocation **2** as solid and in CH_2Cl_2 solution exhibit an isotropic signal (Figure S18, Supporting Information). The g_{iso} value of 2.004/2.005 is in excellent agreement with the notion that the unpaired electron resides on the ligand in a π^* orbital. This is further supported by the fact that the DFT-calculated spin-density (Figure 5) is mainly located on the ligand (97% total spin-density and 23% on iminosemiquinonate nitrogen). Hyperfine-coupling with neighboring atoms like ^{14}N, ^{105}Pd, and ^{1}H nuclei is observed only in CH_2Cl_2−toluene (1:1; v/v) glass (77 K) (Figure 7a). This spectrum could be satisfactorily simulated: g_x = 2.011 (1.9938), g_y = 2.0082 (2.0119), g_z = 1.9855 (2.0058); A^{H1}_{iso}= −3.00 (−2.40), A^{H2}_{iso}= 0.50 (0.42), A^{H3}_{iso}= −2.00 (−1.96), A^{H4}_{iso}= 0.95 (0.91), A^{H5}_{iso}= −2.20 (−2.10), A^{H6}_{iso}= 0.80 (0.77), A^{Pd}_{iso}= 0.90 (0.0), $A^{N}_{(xx)}$ = 12.00 (−0.14), $A^{N}_{(yy)}$= 2.00 (−0.005), $A^{N}_{(zz)}$= 12.00 (11.12). The simulated parameters are comparable with the DFT-calculated values given in the parentheses, except for the hyperfine-interaction value of ^{14}N (iminosemiquinonate nitrogen). A similar observation was encountered earlier.[19c] The monocationic **5** with PPh_3 adduct, which is electronically closely similar to **2**, also exhibits an isotropic signal in the solid state at both 298 and 120 K, with g_{iso} value of 2.005 (Figure S19, Supporting

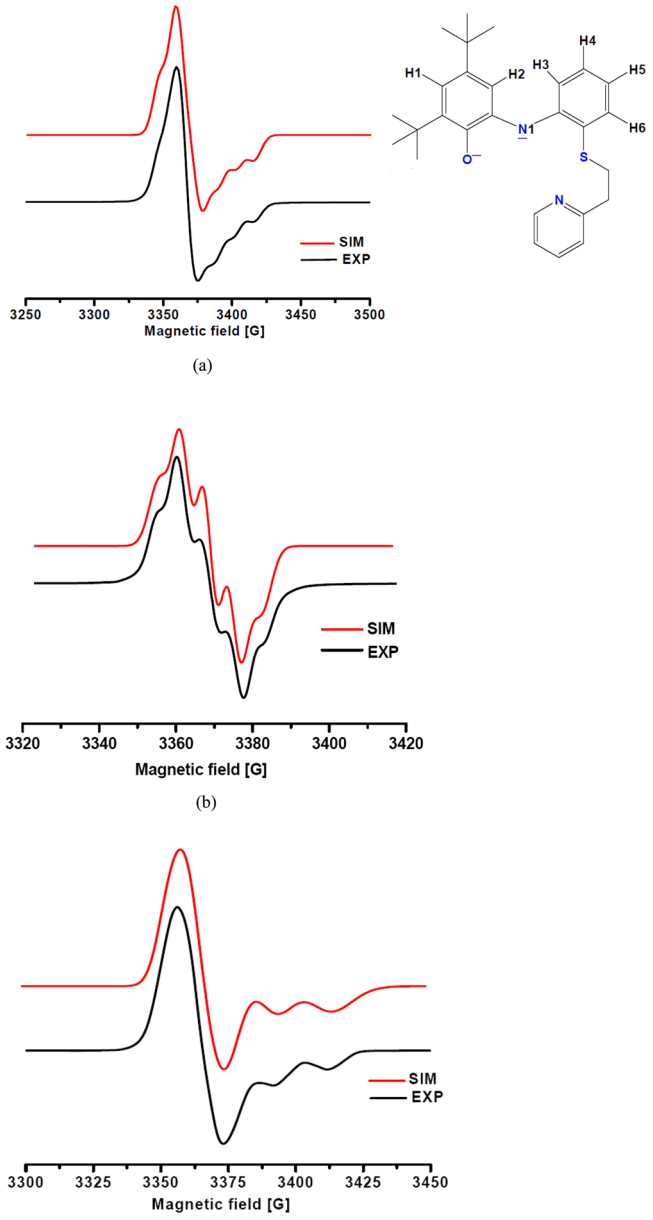

Figure 7. (a) Lower trace: X-band EPR spectrum (77 K) recorded for $[Pd^{II}\{(L^{ISQ})^{\bullet-}\}][PF_6]\cdot CH_2Cl_2$ **2** (*O,N,S,N*-coordination) in CH_2Cl_2−toluene (1:1; v/v) glass (77 K). Upper trace: Simulated EPR spectrum (parameters in the text). (b) Lower trace: X-band EPR spectrum recorded for $[Pd^{II}\{(L^{ISQ})^{\bullet-}\}(PPh_3)][PF_6]\cdot CH_2Cl_2$ **5** (*O,N,N,P*-coordination) in CH_2Cl_2 at 298 K. Upper trace: Simulated EPR spectrum (parameters in the text). (c) Lower trace: X-band EPR spectrum recorded for $[Pd^{II}\{(L^{ISQ})^{\bullet-}\}(PPh_3)][PF_6]\cdot CH_2Cl_2$ **5** (*O,N,N,P*-coordination) in CH_2Cl_2−toluene (1:1; v/v) glass (77 K). Upper trace: Simulated EPR spectrum (parameters in the text).

Information). This is consistent with DFT-calculated spin-density (Figure 6) values (98.5% of total spin-density resides on the ligand, and iminobenzosemiquinonate(1−) nitrogen contributes 36% of the total spin-density). This observation confirms the existence of monoanionic *o*-iminobenzosemiquinonate(1−) π-radical coordinated to Pd center. For **5**, hyperfine-interactions with the surrounding atoms ^{14}N, ^{31}P, and ^{1}H nuclei are observed in CH_2Cl_2 solution at 298 K (Figure 7b). The simulated and DFT-computed (in

DOI: 10.1021/ic503103e
Inorg. Chem. 2015, 54, 5182−5194

parentheses) hyperfine-coupling constant and g values are as follows: $A^{H1}_{iso} = -5.0$ (−4.11), $A^{H2}_{iso} = -1.00$ (−0.99), $A^{N}_{iso} = 6.00$ (5.62), $A^{P}_{iso} = -5.62$ (−6.34), and $g_{iso} = 2.0034$ (2.0021). Complex **5** exhibits an isotropic signal in CH_2Cl_2 at 120 K (Figure S18, Supporting Information). However, in CH_2Cl_2−toluene (1:1; v/v) glass (77 K) (Figure 7c) a hyperfine interaction with surrounding ^{14}N could be observed. The simulated and DFT-calculated (in parentheses) parameters for this spectrum are as follows: $g_x = 2.0118$ (1.9899), $g_y = 2.0057$ (2.0057), $g_z = 1.980$ (2.0108), $A^{N}_{iso} = 4.00$ (5.62).

Absorption Spectra and TD-DFT Results. The electronic spectra of the parent complex $[Pd^{II}\{(L^{AP})^{2-}\}]$ **1**, and of its monocationic and dicationic forms (**2** and **3**, respectively), in which the coordinated ligands are present as *o*-iminobenzosemiquinonate(1−) π-radical $(L^{ISQ})^{\bullet-}$ and *o*-iminobenzoquinone $(L^{IBQ})^{0}$ forms, respectively, are very informative with respect to their electronic structures. The spectra of $[Pd^{II}\{(L^{AP}_{O,N,S,N})^{2-}\}]$ **1**, $[Pd^{II}\{(L^{ISQ}_{O,N,S,N})^{\bullet-}\}]^{1+}$ **2**, and $[Pd^{II}\{(L^{IBQ}_{O,N,S,N})^{0}\}]^{2+}$ **3**, and $[Pd^{II}\{(LISQ)^{\bullet-}\}(PPh_3)][PF_6]\cdot CH_2Cl_2$ **5** are shown in Figure 8. The absorptions are

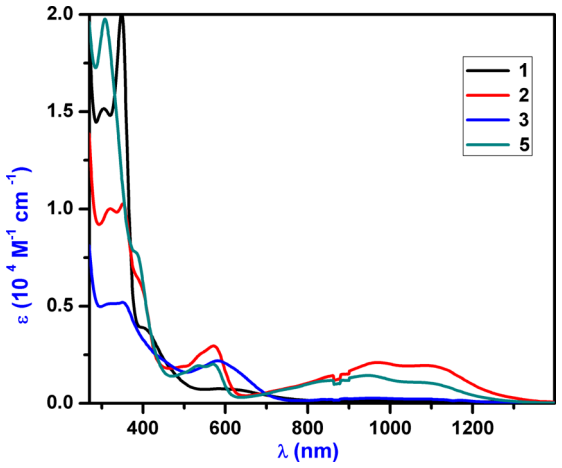

Figure 8. Electronic absorption spectra of $[Pd^{II}\{(L^{AP})^{2-}\}]$ **1**, $[Pd^{II}\{(L^{ISQ})^{\bullet-}\}][PF_6]\cdot CH_2Cl_2$ **2**, $[Pd^{II}\{(L^{IBQ})^{0}\}][BF_4]_2\cdot 2CH_2Cl_2$ **3**, and $[Pd^{II}\{(L^{ISQ})^{\bullet-}\}(PPh_3)][PF_6]\cdot CH_2Cl_2$ **5** in CH_2Cl_2.

dominated by relatively intense distinct transitions due to a spin- and dipole-allowed charge-transfer transition in square-planar Pd^{II} complexes, in which the coordinated ligands are present in its three oxidation levels.[20f,k]

TD-DFT calculations were done on **1**, $[\mathbf{1}]^{1+}$, $[\mathbf{1}]^{2+}$, and **5** to get information about the origin of observed absorptions and to look for a trend within this series of complexes, varying the oxidation level of the coordinated ligands but keeping the oxidation state of the metal (Pd^{II}) invariant. In absorption spectroscopy, complex **1** displays in CH_2Cl_2 characteristic absorptions in the 300−650 nm region: 303 (ε = 15 050 M^{-1} cm^{-1}), 348 (20 050), 406 (3900), 610 (730). TD-DFT calculations on **1** revealed [Figure S20 (cf. Figure 8), Figure S21, and Table S7, Supporting Information] that the low-energy transition calculated at 530 nm involves excitation from (α/β)-HOMO to (α/β)-LUMO and (α/β)-LUMO + 1. Inspection of frontier orbitals shows that this absorption corresponds to a combination of intraligand (amidophenolate-to-ligand pyridine/aminothioetherpyridine) charge-transfer (ILCT), along with ligand-to-metal charge-transfer (LMCT) transition. This indicates that the experimentally observed transition at 610 nm could be a combination of ILCT and LMCT. The origin of experimentally observed transitions in 348 and 406 nm could be correlated to the TD-DFT calculated absorptions at 454 and 345 nm, which could be assigned as transitions ((α/β)-HOMO to (α/β)-LUMO + 2 and (α/β)-HOMO to (α/β)-LUMO + 4) from donor amidophenolate to the acceptor aminothioether moiety and phenolate ring, respectively.

Upon one-electron oxidation, complex **2**/$[\mathbf{1}]^{1+}$ in CH_2Cl_2 solution exhibits absorption maxima at 395 sh (ε = 6110 M^{-1} cm^{-1}), 542 sh (2600), 574 (2900), and two overlapping broad absorptions at 960 (2120) and 1120 nm (1900 M^{-1} cm^{-1}). TD-DFT calculation reveals that the transition in the NIR region (computed as 928 nm) corresponds to β-HOMO to β-LUMO transition [Figure S20 (cf. Figure 8), Figure S22, and Table S8, Supporting Information]. This is associated with intraligand charge-transfer in the iminosemiquinone ring. The transition at ∼550 nm corresponds to β-HOMO − 1/β-HOMO − 2 to β-LUMO. This absorption has significant contribution from the metal-to-ligand charge-transfer (MLCT) component; however, the major contribution seems to be associated with charge-transfer in the iminosemiquinone part. The other transition at ∼400 nm involves β-HOMO − 5/β-HOMO − 4 to β-LUMO transitions which are dominated by mainly a MLCT transition. The MLCT transitions occurring in this case involve charge-transfer from palladium to the electron-deficient iminosemiquinone part of the ligand. Other experimentally observed transitions in the <400 nm region [318 (ε = 9930 M^{-1} cm^{-1}) and 349 (10 150)] can be correlated to the TD-DFT calculated transitions at 305 and 336 nm, respectively. These absorptions are mainly associated with the intraligand charge-transfer from iminosemiquinonate and iminobenzosemiquinonate rings to the pyridine ring.

Upon two-electron oxidation, complex **3**/$[\mathbf{1}]^{2+}$ displays in CH_2Cl_2 solution a characteristic feature at 582 nm (ε = 2230 M^{-1} cm^{-1}) with a shoulder at 450 (2200). From TD-DFT calculation it is observed that the lowest energy absorption (calculated as 652 nm) is due to intraligand charge-transfer in the iminoquinone ring, involving transitions from (α/β) HOMO to (α/β)-LUMO [Figure S20 (cf. Figure 8), Figure S23, and Table S9, Supporting Information]. The transition at 430 nm (consistent with experimentally observed transition at 450 nm) is primarily due to benzoquinone ring to amidobenzoquinone charge-tranfer along with MLCT, involving α-HOMO − 4/β-HOMO − 4 to α-LUMO. Other higher energy broad overlapping transitions could be attributed to intraligand amidobenzoquinone, along with MLCT.

Complex **5** exhibits absorptions similar to those observed for **2**: 386 (ε = 7560 M^{-1} cm^{-1}), 532 (1900), 573 (2050), 950 (1450), 1120 (1050), 308 (19 720) nm. TD-DFT derived transitions are calculated at 758, 566, 398, and 312 nm [Figure S20 (cf. Figure 8), Figure S24, and Table S10, Supporting Information]. Interpretation of the origin of these transitions is similar to that of complex **2**.

The predicted absorption data (Figure S20, Supporting Information), obtained by TD-DFT calculations, reproduce reasonably well the gross features of the observed absorption spectra (cf. Figure 5). Given the fact that absorption spectra of transition-metal complexes is by far the most difficult to calculate by DFT methods, we admit that the remarks made in this section are highly speculative in nature.[33]

DOI: 10.1021/ic503103e
Inorg. Chem. 2015, 54, 5182−5194

SUMMARY AND CONCLUDING REMARKS

In summary, four mononuclear square-planar palladium(II) complexes containing a tetradentate ligand comprising a redox-active *O,N*-coordinated 2-anilino-4,6-di-*tert*-butylphenolate part and supposedly a redox-inactive *S,N*-coordinated ([2′-phenylthio]ethyl)pyridine part have been isolated. Three complexes have been structurally characterized ($Pd^{II}ONSN$ coordination). The complexes belong to a family of three-member ligand-based electron-transfer series. The reactivity potential of three square-planar Pd^{II} complexes with $Pd^{II}ONSN$ coordination (ligands are present in three different redox levels, dianionic, iminosemiquinone, and iminoquinone) toward an externally added ligand PPh_3 has been investigated. Coordination flexibility has been identified in the isolation of complexes with $Pd^{II}ONSP$ and $Pd^{II}ONNP$ coordination. The latter one has been structurally characterized. Crystal structure analysis at 100(2) K has established unambiguously the oxidation level of the redox-active part of the coordinated ligand. The neutral complex is assigned as $[Pd^{II}\{(L^{AP})^{2-}\}]$ ($S = 0$) with a closed-shell *o*-amidophenolato(2−) dianion $(L^{AP})^{2-}$. The monocation and the dication have been assigned as $[Pd^{II}\{(L^{ISQ})^{\bullet-}\}][PF_6]\cdot CH_2Cl_2$ ($S = {}^1/_2$) and $[Pd^{II}\{(L^{IBQ})^0\}][BF_4]_2\cdot 2CH_2Cl_2$ ($S = 0$) containing an *o*-iminobenzosemiquinonate(1−) $(L^{ISQ})^{\bullet-}$ π radical and a closed-shell *o*-iminobenzoquinone $(L^{IBQ})^0$, respectively. The monocationic PPh_3-adduct complex has been assigned as $[Pd^{II}\{(L^{ISQ})^{\bullet-}\}(PPh_3)][PF_6]\cdot CH_2Cl_2$ ($S = {}^1/_2$). The paramagnetic ligand-radical-coordinated complexes display anisotropic EPR spectra. DFT calculations have provided insight into the electronic structure of the complexes. The radical resides on the ligands which are bound to a spectroscopically innocent Pd^{II} ion. The observed switch-over of coordination site flexibility points toward a substrate-binding capability, expected during a catalytic reaction.[13d,25a,50] Explorations of such studies and also the coordination behavior of this new tetradentate ligand toward other transition-metal ions are being carried out in our laboratories.

ASSOCIATED CONTENT

Supporting Information

^1H NMR and ESI-MS spectra of H_2L (Figures S1 and S2, respectively); ^1H NMR spectrum of [Pd(L)] **1** (Figure S3); positive ESI-MS spectrum of **1** {[Pd(L)] + H^+} (Figure S4); ^1H NMR spectrum of $[Pd(L)][BF_4]_2\cdot 2CH_2Cl_2$ **3** (Figure S5); positive ESI-MS spectra of $[Pd(L)]^+$, $\{[Pd(L)]^{2+} + e^-\}^+$ (Figures S6 and S7, respectively); CV scans of $[Pd(L)][PF_6]$ **2** and **3** in CH_2Cl_2 (Figures S8 and S9, respectively); ^1H NMR spectrum of $[Pd(L)(PPh_3)]$ **4** (Figure S10); positive ESI-MS spectrum of $\{[Pd(L)(PPh_3)] + [H^+]\}$ (Figure S11); CV of **4** (Figure S12); ESI-MS spectrum of $\{[Pd(L)(PPh_3)]^+\}$ (Figure S13); XRPD patterns for **1**−**3** and $[Pd^{II}\{(L^{ISQ})^{\bullet-}\}(PPh_3)][PF_6]\cdot CH_2Cl_2$ **5** (Figures S14−17); EPR spectra of **2** (solid and CH_2Cl_2 solution) at 298 and 120 K (Figure S18); EPR spectra of **5** (solid and CH_2Cl_2 solution) at 298 and 120 K (Figure S19); TD-DFT-calculated electronic spectra of $[Pd^{II}\{(L^{AP})^{2-}\}]$ **1**, $[\mathbf{1}]^{1+}$, $[\mathbf{1}]^{2+}$, and **5** (Figure S20); representative molecular orbitals of **1**, $[\mathbf{1}]^{1+}$, $[\mathbf{1}]^{2+}$, and **5** (Figures S21−S24); DFT-optimized Cartesian coordinates and X-ray structural and DFT-optimized bond lengths of **1** (Tables S1 and S2, respectively), $[\mathbf{1}]^{1+}$ (Tables S3 and S2, respectively), $[\mathbf{1}]^{2+}$ (Tables S4 and S2, respectively), and $[Pd(L)(PPh_3)]^{1+}$ (Tables S5 and S6, respectively); TD-DFT-calculated electronic transitions of **1**, $[\mathbf{1}]^{1+}$, $[\mathbf{1}]^{2+}$, and **5** (Tables S7−S10, respectively). Crystallographic data in CIF format. The Supporting Information is available free of charge on the ACS Publications website at DOI: 10.1021/ic503103e.

AUTHOR INFORMATION

Corresponding Author

*E-mail: rnm@iitk.ac.in. Phone: +91-512-2597437. Fax: +91-512-2597436.

Notes

The authors declare no competing financial interest.

ACKNOWLEDGMENTS

This work is supported by the Department of Science & Technology (DST), Government of India. R.M. sincerely thanks DST for a J.C. Bose fellowship. A.A. gratefully acknowledges the award of an SRF by Council of Scientific & Industrial Research (CSIR), Government of India, and S.K.B. acknowledges the award of an SRF by CSIR and a postdoctoral fellowship by IISER Kolkata. We are grateful to Prof. P. K. Bharadwaj of IIT Kanpur and Dr. Sukanta Mandal of IIT Kharagpur for their help in the structure determination of 1 and in simulating EPR spectra and calculating hyperfine interaction parameters. Comments from the reviewers were very helpful at the revision stage.

REFERENCES

(1) (a) Chirik, P. J. *Inorg. Chem.* **2011**, *50*, 9737−9740. (b) Kaim, W. *Inorg. Chem.* **2011**, *50*, 9752−9765.

(2) (a) Limberg, C. *Angew. Chem., Int. Ed.* **2003**, *42*, 5932−5954. (b) Chirik, P. J.; Wieghardt, K. *Science* **2010**, *327*, 794−795. (c) Praneeth, V. K. K.; Ringenberg, M. R.; Ward, T. R. *Angew. Chem., Int. Ed.* **2012**, *51*, 10228−10234. (d) Luca, O. R.; Crabtree, R. H. *Chem. Soc. Rev.* **2013**, *42*, 1440−1459.

(3) (a) Stubbe, J.; van der Donk, W. A. *Chem. Rev.* **1998**, *98*, 705−762. (b) Pierre, J.-L. *Chem. Soc. Rev.* **2000**, *29*, 251−257. (c) Whittaker, J. W. *Chem. Rev.* **2003**, *103*, 2347−2363. (d) Stubbe, J. *Chem. Commun.* **2003**, 2511−2513. (e) Gamez, P.; Koval, I. A.; Reedijk, J. *Dalton Trans.* **2004**, 4079−4088. (f) Chaudhuri, P.; Wieghardt, K.; Weyhermüller, T.; Paine, T. K.; Mukherjee, S.; Mukherjee, C. *Biol. Chem.* **2005**, *386*, 1023−1033. (g) Kaim, W.; Schwederski, B. *Coord. Chem. Rev.* **2010**, *254*, 1580−1588.

(4) (a) Jazdzewski, B. A.; Tolman, W. B. *Coord. Chem. Rev.* **2000**, *200*−*202*, 633−685. (b) Itoh, S.; Taki, M.; Fukuzumi, S. *Coord. Chem. Rev.* **2000**, *198*, 3−20. (c) Thomas, F. *Eur. J. Inorg. Chem.* **2007**, 2379−2404. (d) Lyons, C. T.; Stack, T. D. P. *Coord. Chem. Rev.* **2013**, *257*, 528−540.

(5) (a) Bittner, M. M.; Lindeman, S. V.; Fiedler, A. T. *J. Am. Chem. Soc.* **2012**, *134*, 5460−5463. (b) Bittner, M. M.; Kraus, D.; Lindeman, S. V.; Popescu, C. V.; Fiedler, A. T. *Chem.−Eur. J.* **2013**, *19*, 9686−9698.

(6) Kallol Ray, K.; Petrenko, T.; Wieghardt, K.; Neese, F. *Dalton Trans.* **2007**, 1552−1566.

(7) Butin, K. P.; Beloglazkina, E. K.; Zyk, N. V. *Russ. Chem. Rev.* **2005**, *74*, 531−553.

(8) Pierpont, C. G.; Buchanan, R. M. *Coord. Chem. Rev.* **1981**, *38*, 45−87. (b) Pierpont, C. G.; Lange, C. W. *Prog. Inorg. Chem.* **1994**, *41*, 331−442. (c) Pierpont, C. G. *Coord. Chem. Rev.* **2001**, *216*−*217*, 99−125. (d) Pierpont, C. G. *Coord. Chem. Rev.* **2001**, *219*−*221*, 415−433. Pierpont, C. G. *Inorg. Chem.* **2011**, *50*, 9766−9772.

(9) Lever, A. B. P.; Masui, H.; Metcalfe, R. A.; Stufkens, D. J.; Dodsworth, E. S.; Auburn, P. R. *Coord. Chem. Rev.* **1993**, *125*, 317−332.

(10) (a) Ward, M. D.; McCleverty, J. A. *J. Chem. Soc., Dalton Trans.* **2002**, 275−288. (b) Sproules, S.; Wieghardt, K. *Coord. Chem. Rev.* **2010**, *254*, 1358−1382.

DOI: 10.1021/ic503103e
Inorg. Chem. 2015, 54, 5182−5194

(11) Chaudhuri, P.; Wieghardt, K. *Prog. Inorg. Chem.* **2001**, *50*, 151−216.
(12) (a) Patra, A. K.; Ray, M.; Mukherjee, R. *Inorg. Chem.* **2000**, *39*, 652−657. (b) Dutta, S. K.; Beckmann, U.; Bill, E.; Weyhermüller, T.; Wieghardt, K. *Inorg. Chem.* **2000**, *39*, 3355−3364.
(13) (a) Noro, S.-i.; Chang, H.-C.; Takenobu, T.; Murayama, Y.; Kanbara, T.; Aoyama, T.; Sassa, T.; Wada, T.; Tanaka, D.; Kitagawa, S.; Iwasa, Y.; Akutagawa, T.; Nakamura, T. *J. Am. Chem. Soc.* **2005**, *127*, 10012−10013. (b) Khusniyarov, M. M.; Harms, K.; Burghaus, O.; Sundermeyer, J.; Sarkar, B.; Kaim, W.; van Slageren, J.; Duboc, C.; Fiedler, J. *Dalton Trans.* **2008**, 1355−1365 and references therein. (c) Khusniyarov, M. M.; Bill, E.; Weyhermüller, T.; Bothe, E.; Harms, K.; Sundermeyer, J.; Wieghardt, K. *Chem.−Eur. J.* **2008**, *14*, 7608−7622. (d) van der Meer, M.; Rechkemmer, Y.; Peremykin, I.; Hohloch, S.; van Slageren, J.; Sarkar, B. *Chem. Commun.* **2014**, *50*, 11104−11106.
(14) (a) Pratt, R. C.; Stack, T. D. P. *J. Am. Chem. Soc.* **2003**, *125*, 8716−8717. (b) Pratt, R. C.; Mirica, L. M.; Stack, T. D. P. *Inorg. Chem.* **2004**, *43*, 8030−8039. (c) Storr, T.; Wasinger, E. C.; Pratt, R. C.; Stack, T. D. P. *Angew. Chem., Int. Ed.* **2007**, *46*, 5198−5201. (d) Storr, T.; Verma, P.; Pratt, R. C.; Wasinger, E. C.; Shimazaki, Y.; Stack, T. D. P. *J. Am. Chem. Soc.* **2008**, *130*, 15448−15459. (e) Storr, T.; Verma, P.; Shimazaki, Y.; Wasinger, E. C.; Stack, T. D. P. *Chem.−Eur. J.* **2010**, *16*, 8980−8983. (f) Verma, P.; Pratt, R. C.; Storr, T.; Wasinger, E. C.; Stack, T. D. P. *Proc. Natl. Acad. Sci. U.S.A.* **2011**, *108*, 18600−18605. (g) Pratt, R. C.; Lyons, C. T.; Wasinger, E. C.; Stack, T. D. P. *J. Am. Chem. Soc.* **2012**, *134*, 7367−7377.
(15) (a) Rotthaus, O.; Jarjayes, O.; Thomas, F.; Philouze, C.; Valle, C. P. D.; Saint-Aman, E.; Pierre, J.-L. *Chem.−Eur. J.* **2006**, *12*, 2293−2302. (b) Rotthaus, O.; Thomas, F.; Jarjayes, O.; Philouze, C.; Saint-Aman, E.; Pierre, J.-L. *Chem.−Eur. J.* **2006**, *12*, 6953−6962. (c) Rotthaus, O.; Jarjayes, O.; Valle, C. P. D.; Philouze, C.; Thomas, F. *Chem. Commun.* **2007**, 4462−4464. (d) Rotthaus, O.; Jarjayes, O.; Philouze, C.; Del Valle, C. P.; Thomas, F. *Dalton Trans.* **2009**, 1792−1800. (e) Orio, M.; Philouze, C.; Jarjayes, O.; Neese, F.; Thomas, F. *Inorg. Chem.* **2010**, *49*, 646−658. (f) Orio, M.; Jarjayes, O.; Kanso, H.; Philouze, C.; Neese, F.; Thomas, F. *Angew. Chem., Int. Ed.* **2010**, *49*, 4989−4992. (g) Kochem, A.; Jarjayes, O.; Baptiste, B.; Philouze, C.; Vezin, H.; Tsukidate, K.; Tani, F.; Orio, M.; Shimazaki, Y.; Thomas, F. *Chem.−Eur. J.* **2012**, *18*, 1068−1072. (h) Kochem, A.; Kanso, H.; Baptiste, B.; Arora, H.; Philouze, C.; Jarjayes, O.; Vezin, H.; Luneau, D.; Orio, M.; Thomas, F. *Inorg. Chem.* **2012**, *51*, 10557−10571.
(16) (a) Shimazaki, Y.; Huth, S.; Hirota, S.; Yamauchi, O. *Bull. Chem. Soc., Jpn.* **2000**, *73*, 1187−1195. (b) Shimazaki, Y.; Tani, F.; Fukui, K.; Naruta, Y.; Yamauchi, O. *J. Am. Chem. Soc.* **2003**, *125*, 10512−10513. (c) Yuichi Shimazaki, Y.; Huth, S.; Karasawa, S.; Hirota, S.; Naruta, Y.; Yamauchi, O. *Inorg. Chem.* **2004**, *43*, 7816−7822. (d) Shimazaki, Y.; Yajima, T.; Tani, F.; Karasawa, S.; Fukui, K.; Naruta, Y.; Yamauchi, O. *J. Am. Chem. Soc.* **2007**, *129*, 2559−2568. (e) Shimazaki, Y.; Kabe, R.; Huth, S.; Tani, F.; Naruta, Y.; Yamauchi, O. *Inorg. Chem.* **2007**, *46*, 6083−6090. (f) Shimazaki, Y.; Yajima, T.; Shiraiwa, T.; Yamauchi, O. *Inorg. Chim. Acta* **2009**, *362*, 2467−2474. (g) Shimazaki, Y.; Yamauchi, O. *Indian J. Chem.* **2011**, *50A*, 383−394. (h) Shimazaki, Y.; Arai, N.; Dunn, T. J.; Yajima, T.; Tani, F.; Ramogida, C. F.; Storr, T. *Dalton Trans.* **2011**, *40*, 2469−2479. (i) Dunn, T. J.; Ramogida, C. F.; Simmonds, C.; Paterson, A.; Wong, E. W. Y.; Chiang, L.; Shimazaki, Y.; Storr, T. *Inorg. Chem.* **2011**, *50*, 6746−6755. (j) Dunn, T. J.; Chiang, L.; Ramogida, C. F.; Webb, M. I.; Savard, D.; Sakaguchi, M.; Ogura, T.; Shimazaki, Y.; Storr, T. *Dalton Trans.* **2012**, *41*, 7905−7914. (k) Dunn, T. J.; Webb, M. I.; Hazin, K.; Verma, P.; Wasinger, E. C.; Shimazaki, Y.; Storr, T. *Dalton Trans.* **2013**, *42*, 3950−3956. (l) Balaghi, S. E.; Safaei, E.; Chiang, L.; Wong, E. W. Y.; Savard, D.; Clarke, R. M.; Storr, T. *Dalton Trans.* **2013**, *42*, 6829−6839. (m) Asami, K.; Takashina, A.; Kobayashi, M.; Iwatsuki, S.; Yajima, T.; Kochem, A.; van Gastel, M.; Tani, F.; Kohzuma, T.; Thomas, F.; Shimazaki, Y. *Dalton Trans.* **2014**, *43*, 2283−2293.
(17) (a) Stenson, P. A.; Board, A.; Marin-Becerra, A.; Blake, A. J.; Davies, E. S.; Wilson, C.; McMaster, J.; Schröder, M. *Chem.−Eur. J.* **2008**, *14*, 2564−2576. (b) Franks, M.; Gadzhieva, A.; Ghandhi, L.; Murrell, D.; Blake, A. J.; Davies, E. S.; Lewis, W.; Moro, F.; McMaster, J.; Schröder, M. *Inorg. Chem.* **2013**, *52*, 660−670. (c) Eckshtain-Levi, M.; Orio, M.; Lavi, R.; Benisvy, L. *Dalton Trans.* **2013**, *42*, 13323−13326.
(18) (a) Poddel'sky, A. I.; Cherkasov, V. K.; Abakumov, G. A. *Coord. Chem. Rev.* **2009**, *253*, 291−324.
(19) (a) Broere, D. L. J.; de Bruin, B.; Reek, J. N. H.; Lutz, M.; Dechert, S.; van der Vlugt, J. I. *J. Am. Chem. Soc.* **2014**, *136*, 11574−11577. (b) Sanz, C. A.; Ferguson, M. J.; McDonald, R.; Patrick, B. O.; Hicks, R. G. *Chem. Commun.* **2014**, *50*, 11676−11678. (c) Broere, D. L. J.; Metz, L. L.; de Bruin, B.; Reek, J. N. H.; Siegler, M. A.; van der Vlugt, J. I. *Angew. Chem., Int. Ed.* **2015**, *54*, 1516−1520.
(20) (a) Chaudhuri, P.; Verani, C. N.; Bill, E.; Bothe, E.; Weyhermüller, T.; Wieghardt, K. *J. Am. Chem. Soc.* **2001**, *123*, 2213−2223. (b) Chun, H.; Verani, C.; Chaudhuri, P.; Bothe, E.; Bill, E.; Weyhermüller, T.; Wieghardt, K. *Inorg. Chem.* **2001**, *40*, 4157−4166. (c) Chun, H.; Chaudhuri, P.; Weyhermüller, T.; Wieghardt, K. *Inorg. Chem.* **2002**, *41*, 790−795. (d) Herebian, D.; Ghosh, P.; Chun, H.; Bothe, E.; Weyhermüller, T.; Wieghardt, K. *Eur. J. Inorg. Chem.* **2002**, 1957−1967. (e) Bachler, V.; Olbrich, G.; Neese, F.; Wieghardt, K. *Inorg. Chem.* **2002**, *41*, 4179−4193. (f) Sun, X.; Chun, H.; Hildenbrand, K.; Bothe, E.; Weyhermüller, T.; Neese, F.; Wieghardt, K. *Inorg. Chem.* **2002**, *41*, 4295−4303. (g) Min, K. S.; Weyhermüller, T.; Wieghardt, K. *Dalton Trans.* **2003**, 1126−1132. (h) Min, K. S.; Weyhermüller, T.; Bothe, E.; Wieghardt, K. *Inorg. Chem.* **2004**, *43*, 2922−2931. (i) Bill, E.; Bothe, E.; Chaudhuri, P.; Chlopek, K.; Herebian, D.; Kokatam, S.; Ray, K.; Weyhermüller, T.; Neese, F.; Wieghardt, K. *Chem.−Eur. J.* **2005**, *11*, 204−224. (j) Mukherjee, S.; Weyhermüller, T.; Bill, E.; Wieghardt, K.; Chaudhuri, P. *Inorg. Chem.* **2005**, *44*, 7099−7108. (k) Kokatam, S.-L.; Chaudhuri, P.; Weyhermüller, T.; Wieghardt, K. *Dalton Trans.* **2007**, 373−378.
(21) (a) Saha Roy, A.; Saha, P.; Das Adhikary, N.; Ghosh, P. *Inorg. Chem.* **2011**, *50*, 2488−2500. (b) Ghorai, S.; Mukherjee, C. *Dalton Trans.* **2014**, *43*, 394−397. (c) Rakshit, R.; Ghorai, S.; Biswas, S.; Mukherjee, C. *Inorg. Chem.* **2014**, *53*, 3333−3337.
(22) (a) Ye, S.; Sarkar, B.; Lissner, F.; Schleid, T.; van Slageren, J.; Fiedler, J.; Kaim, W. *Angew. Chem., Int. Ed.* **2005**, *44*, 2103−2106. (b) Das, D.; Mondal, T. K.; Dutta Chowdhury, A.; Weisser, F.; Schweinfurth, D.; Sarkar, B.; Mobin, S. M.; Urbanos, F. A.; Jiménez-Aparicio, R.; Lahiri, G. K. *Dalton Trans.* **2011**, *40*, 8377−8390 and references therein. (c) Das, D.; Scherer, T. M.; Das, A.; Mondal, T. K.; Mobin, S. M.; Fiedler, J.; Priego, J. L.; Jiménez-Aparicio, R.; Kaim, W.; Lahiri, G. K. *Dalton Trans.* **2012**, *41*, 11675−11683. (d) Das, D.; Agarwala, H.; Dutta Chowdhury, A.; Patra, T.; Mobin, S. M.; Sarkar, B.; Kaim, W.; Lahiri, G. K. *Chem. Eur.−J.* **2013**, *19*, 7384−7394.
(23) Piskunov, A. V.; Mescheryakova, I. N.; Fukin, G. K.; Baranov, E. V.; Hummert, M.; Shavyrin, A. S.; Cherkasov, V. K.; Abakumov, G. A. *Chem.−Eur. J.* **2008**, *14*, 10085−10093.
(24) (a) Kopec, J. A.; Shekar, S.; Brown, S. N. *Inorg. Chem.* **2012**, *51*, 1239−1250. (b) Brown, S. N. *Inorg. Chem.* **2012**, *51*, 1251−1260. (c) Shekar, S.; Brown, S. N. *Dalton Trans.* **2014**, *43*, 3601−3611.
(25) (a) Deibel, N.; Schweinfurth, D.; Hohloch, S.; Fiedler, J.; Sarkar, B. *Chem. Commun.* **2012**, *48*, 2388−2390. (b) Deibel, N.; Schweinfurth, D.; Hohloch, S.; Delor, M.; Sazanovich, I. V.; Towrie, M.; Weinstein, J. A.; Sarkar, B. *Inorg. Chem.* **2014**, *53*, 1021−1031.
(26) (a) Gibson, V. C.; Redshaw, C.; Solan, G. A. *Chem. Rev.* **2007**, *107*, 1745−1776. (b) Manuel, T. D.; Rohde, J.-U. *J. Am. Chem. Soc.* **2009**, *131*, 15582−15583.
(27) Samanta, S.; Ghosh, P.; Goswami, S. *Dalton Trans.* **2012**, *41*, 2213−2226.
(28) Singh, A. K.; Mukherjee, R. *Inorg. Chem.* **2005**, *44*, 5813−5819.
(29) (a) Hicks, R. G. *Angew. Chem., Int. Ed.* **2008**, *47*, 7393−7395. (b) Khusniyarov, M. M.; Bill, E.; Weyhermüller, T.; Bothe, E.; Wieghardt, K. *Angew. Chem., Int. Ed.* **2011**, *50*, 1652−1655.
(30) (a) Blackmore, K. J.; Lal, N.; Ziller, J. W.; Heyduk, A. F. *Eur. J. Inorg. Chem.* **2009**, 735−743. (b) Fedushkin, I. L.; Makarov, V. M.; Sokolov, V. G.; Fukin, G. K. *Dalton Trans.* **2009**, 8047−8053. (c) King, E. R.; Betley, T. A. *J. Am. Chem. Soc.* **2009**, *131*, 14374−14380. (d) Sazama, G. T.; Betley, T. A. *Inorg. Chem.* **2010**, *49*, 2512−2524.

DOI: 10.1021/ic503103e
Inorg. Chem. 2015, 54, 5182−5194

(e) Clark, K. M.; Bendix, J.; Heyduk, A. F.; Ziller, J. W. *Inorg. Chem.* **2012**, *51*, 7457−7459. (f) Butsch, K.; Klein, A.; Nitsche, S.; Stirnat, K.; Hawkett, J. R.; McInnes, E. J. L.; Bauer, M. *Dalton Trans.* **2012**, *41*, 11464−11475. (g) Castellano, M.; Ruiz-García, R.; Cano, J.; Julve, M.; Lloret, F.; Journaux, Y.; De Munno, G.; Armentano, D. *Chem. Commun.* **2013**, *49*, 3534−3536.
(31) (a) Johnston, C. W.; McKinnon, S. D. J.; Patrick, B. O.; Hicks, R. G. *Dalton Trans.* **2013**, *42*, 16829−16836. (b) Morgan, I. S.; Peuronen, A.; Hänninen, M. M.; Reed, R. W.; Clérac, R.; Tuononen, H. M. *Inorg. Chem.* **2014**, *53*, 33−35.
(32) (a) Benisvy, L.; Blake, A. J.; Collison, D.; Davies, E. S.; Garner, C. D.; McInnes, E. J. L.; McMaster, J.; Whittaker, G.; Wilson, C. *Chem. Commun.* **2001**, 1824−1825. (b) Benisvy, L.; Blake, A. J.; Collison, D.; Davies, E. S.; Garner, C. D.; McInnes, E. J. L.; McMaster, J.; Whittaker, G.; Wilson, C. *Dalton Trans.* **2003**, 1975−1985. (c) Benisvy, L.; Bill, E.; Blake, A. J.; Collison, D.; Davies, E. S.; Garner, C. D.; McArdle, G.; McInnes, E. J. L.; McMaster, J.; Ross, S. H. K.; Wilson, C. *Dalton Trans.* **2006**, 258−267. (d) Zats, G. M.; Arora, H.; Lavi, R.; Yufit, D.; Benisvy, L. *Dalton Trans.* **2011**, *40*, 10889−10896. (e) Zats, G. M.; Arora, H.; Lavi, R.; Yufit, D.; Benisvy, L. *Dalton Trans.* **2012**, *41*, 47−49. (f) Jenny-Lee Mathias, J.-L.; Arora, H.; Lavi, R.; Vezin, H.; Yufit, D.; Orio, M.; Aliaga-Alcade, N.; Benisvy, L. *Dalton Trans.* **2013**, *42*, 2358−2361.
(33) Rajput, A.; Sharma, A. K.; Barman, S. K.; Koley, D.; Steinert, M.; Mukherjee, R. *Inorg. Chem.* **2014**, *53*, 36−48 and references therein.
(34) Gilbert, J. G.; Addison, A. W.; Butcher, R. J. *Inorg. Chim. Acta* **2000**, *308*, 22−30.
(35) Ercolani, C.; Gardini, M.; Pennesi, G.; Rossi, G.; Russo, U. *Inorg. Chem.* **1988**, *27*, 422−424.
(36) (a) Ray, M.; Ghosh, D.; Shirin, Z.; Mukherjee, R. *Inorg. Chem.* **1997**, *36*, 3568−3572. (b) Patra, A. K.; Mukherjee, R. *Inorg. Chem.* **1999**, *38*, 1388−1393.
(37) O'Connor, C. J. *Prog. Inorg. Chem.* **1982**, *29*, 203−283.
(38) Evans, D. F. *J. Chem. Soc.* **1959**, 2003−2005.
(39) Farrugia, L. J. *WinGX version 1.64, An Integrated Systems of Windows Programs for the Solution, Refinement and Analysis of Single-Crystal X-ray Diffraction Data*; Department of Chemistry, University of Glasgow: Glasgow, U.K., 2003.
(40) Frisch, M. J.; Trucks, G. W.; Schlegel, H. B.; Scuseria, G. E.; Robb, M. A.; Cheeseman, J. R.; Scalmani, G.; Barone, V.; Mennucci, B.; Petersson, G. A.; Nakatsuji, H.; Caricato, M.; Li, X.; Hratchian, H. P.; Izmaylov, A. F.; Bloino, J.; Zheng, G.; Sonnenberg, J. L.; Hada, M.; Ehara, M.; Toyota, K.; Fukuda, R.; Hasegawa, J.; Ishida, M.; Nakajima, T.; Honda, Y.; Kitao, O.; Nakai, H.; Vreven, T.; Montgomery, J. A., Jr.; Peralta, J. E.; Ogliaro, F.; Bearpark, M.; Heyd, J. J.; Brothers, E.; Kudin, K. N.; Staroverov, V. N.; Kobayashi, R.; Normand, J.; Raghavachari, K.; Rendell, A.; Burant, J. C.; Iyengar, S. S.; Tomasi, J.; Cossi, M.; Rega, N.; Millam, N. J.; Klene, M.; Knox, J. E.; Cross, J. B.; Bakken, V.; Adamo, C.; Jaramillo, J.; Gomperts, R.; Stratmann, R. E.; Yazyev, O.; Austin, A. J.; Cammi, R.; Pomelli, C.; Ochterski, J. W.; Martin, R. L.; Morokuma, K.; Zakrzewski, V. G.; Voth, G. A.; Salvador, P.; Dannenberg, J. J.; Dapprich, S.; Daniels, A. D.; Farkas, Ö.; Foresman, J. B.; Ortiz, J. V.; Cioslowski, J.; Fox, D. J. *Gaussian 09, revision B.01*; Gaussian, Inc.: Wallingford, CT, 2010.
(41) (a) Becke, A. D. *J. Chem. Phys.* **1993**, *98*, 5648−5652. (b) Lee, C.; Yang, W.; Parr, R. G. *Phys. Rev. B* **1988**, *37*, 785−789. (c) Stevens, P. J.; Devlin, F. J.; Chabalowski, C. F.; Frisch, M. *J. Phys. Chem.* **1994**, *98*, 11623−11627.
(42) Hay, P. J.; Wadt, W. R. *J. Chem. Phys.* **1985**, *82*, 270−283.
(43) Schafer, A.; Huber, C.; Ahlrichs, R. *J. Chem. Phys.* **1994**, *100*, 5829−5835.
(44) Schafer, A.; Horn, H.; Ahlrichs, R. *J. Chem. Phys.* **1992**, *97*, 2571−2577.
(45) (a) Barone, V.; Cossi, M. *J. Phys. Chem. A* **1998**, *102*, 1995−2001. (b) Cossi, M.; Barone, V. *J. Chem. Phys.* **2001**, *115*, 4708−4717. (c) Cossi, M.; Rega, N.; Scalmani, G.; Barone, V. *J. Comput. Chem.* **2003**, *24*, 669−681.
(46) O'Boyle, N. M.; Tenderholt, A. L.; Langner, K. M. *J. Comput. Chem.* **2008**, *29*, 839−845.
(47) http://www.chemcraftprog.com/.
(48) O'Mahony, G. E.; Kelly, P.; Lawrence, S. E.; Maguire, A. R. *ARKIVOC* **2011**, No. i, 1−110.
(49) Connelly, N. G.; Geiger, W. E. *Chem. Rev.* **1996**, *96*, 877−910.
(50) Ringenberg, M. R.; Kokatam, S. L.; Heiden, Z. M.; Rauchfuss, T. B. *J. Am. Chem. Soc.* **2008**, *130*, 788−789.

NOTE ADDED IN PROOF

During the preparation of this manuscript, a relevant reference missed out (Metzinger, R.; Demeshko, S.; Limberg, C. *Chem.—Eur. J.* **2014**, *20*, 4721−4735). Notably, this paper describes iron chemistry of a new aminophenol-based pentadentate ligand.

DOI: 10.1021/ic503103e
Inorg. Chem. 2015, 54, 5182−5194